

Theory of self-organized traffic at light signal

Boris S. Kerner ^{1, 2}

¹ *Daimler AG, RD/RTF, HPC: G021, 71059 Sindelfingen, Germany and*

² *Physik von Transport und Verkehr,*

Universität Duisburg-Essen, 47048 Duisburg, Germany

Abstract

Based on numerical simulations of a three-phase traffic flow model, a probabilistic theory of traffic at the light signal is developed. We have found that very complex spatiotemporal self-organized phenomena determine features of city traffic. We have revealed that the breakdown of *green wave* in a city is initiated by the emergence of a moving synchronized flow pattern (MSP) within the green wave. It turns out that a sequence of $F \rightarrow S \rightarrow J$ transitions (F – free flow, S – synchronized flow, J – moving queue) lead to traffic breakdown at the light signal. Both spontaneous and induced breakdowns of the green wave have been found. From a study of a variety of scenarios for arrival traffic, we have found that there are the infinite number of capacities of traffic at the light signal, which are in a capacity range between a minimum capacity and maximum capacity; each of the capacities gives a flow rate at which under-saturated traffic is in a metastable state with respect to the transition to over-saturated traffic. The maximum capacity depends crucially on a time-dependence of the flow rate: The larger the number of vehicles that arrive the light signal during the green phase, the larger the maximum capacity.

PACS numbers: 89.40.-a, 47.54.-r, 64.60.Cn, 05.65.+b

I. INTRODUCTION

Light signals in city intersections act as bottlenecks determining the main features of city traffic. One of the basic characteristics of a well-known Webster model [1] as well as other classical models and theories of traffic at light signal (see [2–14] and reviews [15, 16]) is traffic capacity at the light signal

$$C_{\text{cl}} = q_{\text{sat}} T_{\text{G}}^{(\text{eff})} / \vartheta, \quad (1)$$

where q_{sat} is the saturation flow rate, i.e., the mean flow rate from a vehicle queue at the light signal during green phase when vehicles discharge from the queue to their maximum free speed v_{free} ; $\vartheta = T_{\text{G}} + T_{\text{Y}} + T_{\text{R}}$ is the period (cycle time) of the light signal that is assumed to be constant, T_{G} , T_{Y} , and T_{R} are durations of the green, yellow, and red phases of the light signal, respectively; $T_{\text{G}}^{(\text{eff})}$ is the effective green phase time that is the portion of the cycle time during which vehicles are assumed to pass the light signal at constant rate q_{sat} . A summary of these and other definitions, variables, and values used is given in Appendix A.

In the classical theories (reviews [15, 16]), capacity C_{cl} (1) determines the transition from under- to over-saturated traffic. In under-saturated traffic, all vehicles, which are waiting within a queue during the red phase, can pass the signal during the green phase. An opposite case occurs in over-saturated traffic and, therefore, the queue grows. It is assumed [15, 16] that if $q_{\text{in}} > C_{\text{cl}}$, i.e., capacity (1) is less than the flow rate of vehicles q_{in} that arrive at the light signal (called as arrival traffic rate on the approach [15]), then a transition from under- to over-saturated traffic occurs.

In the classical theories of city traffic is furthermore assumed that no instabilities and no self-organization phenomena can occur in city traffic (reviews [15, 16]). This is because traffic lights should constitute massive deterministic perturbations suppressing the self-organized phenomena in city traffic. This has also been earlier assumed by the author (see Sec. 22.4 in [17] and footnote 1 in Chap. 1 of [18]). In contrast, as the author has recently found, in under-saturated traffic spontaneous traffic breakdown, i.e., the phase transition from under- to over-saturated traffic can occur at the light signal after a random time delay $T^{(\text{B})}$ with some probability $P^{(\text{B})}$ [19]: the queue at the light signal begins to self-grow non-reversibly leading to traffic gridlock.

In this article, based on numerical simulations of a three-phase traffic flow model we present a probabilistic theory of traffic at the light signal. In this theory, features of city

traffic are determined by traffic breakdown and resulting spatiotemporal self-organization traffic phenomena. The classical theories of city traffic are the basis for a variety of light signal control systems, for example, for an arterial progressive control during which vehicles should travel unimpeded in a city [15]; this should implement a well-known idea about a *green wave* in a city. However, we will reveal that complex self-organization traffic phenomena at the light signal should be taken into account for the optimization of a green wave in a city.

The article is organized as follows. In Sec. II, we present a theory of the breakdown of a green wave at an isolated light signal. Self-organization phenomena due to spatiotemporal interaction of the green wave with a vehicle queue are the subject of Sec. III. In Sec. IV, we study probability of traffic breakdown. The infinite number of capacities of traffic at the light signal are considered in Sec. V. Induced breakdown of green wave is studied in Sec. VI. In Sec. VII, we study a diagram of the breakdown at the light signal and show that probability of green wave breakdown can exhibit a minimum as a function of light signal characteristics. Green wave breakdown occurring in a more general case of a sequence of the light signals is discussed in Sec. VIII. A discussion of possible applications of the BM (breakdown minimization) principle for optimization of the green wave in a city is made in Sec. IX. In Sec. X, we make a comparison of traffic breakdown at highway bottleneck and bottleneck due to the light signal (Sec. X A), compare results of three-phase and two-phase traffic flow theories in the application to city traffic (Sec. X B) as well as formulate conclusions.

II. BREAKDOWN OF GREEN WAVE

A. Model of green wave at isolated light signal

In Sec. II, we consider a hypothetical green wave when there is no initial vehicle queue at the light signal. When the green wave propagates through several identical light signals (Fig. 1), probability that spontaneous green wave breakdown occurs in *at least* at one of the light signals is larger than probability $P^{(B)}$ that the breakdown occurs *only* at a chosen light signal. Therefore, firstly to study the physics of self-organized traffic, we consider the propagation of a green wave through an *isolated* light signal at location $x = x_{LS}$ on a single-lane city link. In this model, ΔT_b denotes a time gap between the end of the red phase and

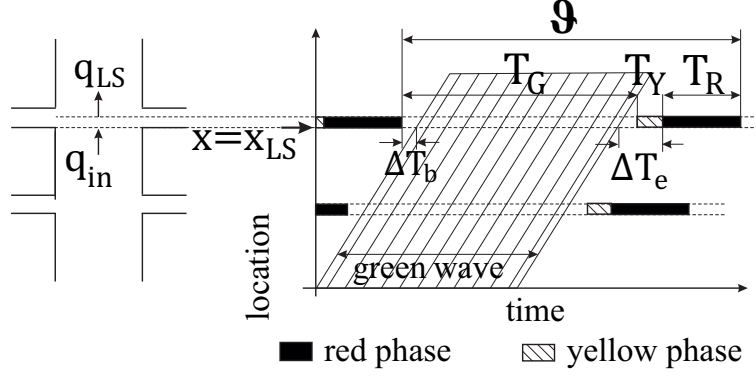


FIG. 1: Model of green wave. q_{in} and q_{LS} are rates of arrival traffic at light signal and in light signal outflow, respectively.

beginning of the green wave; ΔT_e denotes a time gap between the end of the green wave and beginning of the red phase (Fig. 1).

Open boundary conditions have been used in all simulations. For each cycle of the light signal, vehicles are generated at the road beginning $x = x_b$ during a given time interval T_{GW} with random time headways between vehicles that deviate within 10% from a given mean gross time headway τ_{GW} ; the latter determines the flow rate $q_{GW} = 3600/\tau_{GW}$ vehicles/h. The initial vehicle speed is equal to $v_{free} = 55$ km/h. The time interval between the beginning of the time interval T_{GW} and beginning of the green phase for the light signal at location $x = x_{LS}$ is calculated from formula $((x_{LS} - x_b)/v_{free}) - \Delta T_b^{(ideal)}$, where $\Delta T_b^{(ideal)}$ denotes a value ΔT_b under undisturbed and noiseless vehicle motion at the speed v_{free} . Under such a hypothetical vehicle motion, the time gap $\Delta T_e = \Delta T_e^{(ideal)} = T_G + T_Y - T_{GW} - \Delta T_b^{(ideal)}$. After vehicles have passed the light signal, they leave freely the simulation area. Even in this hypothetical model, we reveal the phenomenon of spontaneous breakdown of the green wave. However, before we briefly consider a new feature of Kerner-Klenov microscopic three-phase traffic flow model used for simulations (Sec. II B) as well as features of two basic traffic localized patterns needed for the paper understanding (Sec. II C).

B. Three-phase microscopic stochastic traffic flow model for city traffic

For a study of city traffic we have used a discrete version of the Kerner-Klenov stochastic three-phase microscopic model for a single-lane road whose continuum version has initially

been developed for highway traffic [20, 21] that reads as follows:

$$v_{n+1} = \max(0, \min(v_{\text{free}}, \tilde{v}_{n+1} + \xi_n, v_n + a\tau, v_{s,n})), \quad (2)$$

$$x_{n+1} = x_n + v_{n+1}\tau, \quad (3)$$

where $n = 0, 1, 2, \dots$ is number of time steps, $\tau = 1$ s is a time step [65], x_n and v_n are the vehicle coordinate and speed at time step n , a is the maximum acceleration, v_{free} is a maximum speed in free flow, \tilde{v}_n is the vehicle speed without speed fluctuations ξ_n , $v_{s,n}$ is a safe speed.

In addition to a lower speed v_{free} [19], in city traffic we should ensure a larger vehicle acceleration from a standstill in a queue in comparison with a relatively small acceleration a in (2) chosen in accordance with empirical features of a phase transition from free flow to synchronized flow (F→S transition) [19, 20]. This larger acceleration is required to satisfy an empirical value of lost time during the green phase $\delta t = T_G - T_G^{(\text{eff})} \approx 3\text{--}4$ s [15, 16]. We have made the following model development. When the speed difference $\Delta v_n = v_{\ell,n} - v_n$ between the vehicle speed v_n and speed of the preceding vehicle $v_{\ell,n}$ is great enough and/or the acceleration of the preceding vehicle $a_{\ell,n}$ is large enough satisfying condition

$$\Delta v_n + a_{\ell,n}\tau \geq \Delta v_a, \quad (4)$$

then rather than acceleration a , the larger maximum acceleration $k_a a$ with $k_a > 1$ is used; in (4), Δv_a is constant. Otherwise, the maximum acceleration remains to be equal to a of the original model [19, 20]. Because all other model functions are the same as those in the Kerner-Klenov model for a single-lane road [67, 68], the functions and parameters are given in Appendix B. The physical sense of condition (4) is as follows. If (4) is not satisfied, rules of vehicle motion are the same as those of the initial model [19, 20]. However, when condition (4) is satisfied, rather than car-following within synchronized flow at a small acceleration a , the vehicle follows the preceding vehicle with a greater acceleration $k_a a$ [66]. As a result, the model time lost $\delta t = T_G - T_G^{(\text{eff})} \approx 3.2$ s satisfies empirical values.

As in [19], in the model vehicles decelerate at the upstream front of a queue at the light signal as they do this at the upstream front of a wide moving jam propagating on a road without light signals [17, 18]. During the green phase, vehicles accelerate at the downstream queue front (queue discharge) with a random time delay as they do it at the downstream jam front; in other words, the well-known saturation flow rate of queue discharge is equal to

the jam outflow q_{out} under the condition that vehicles accelerate to the maximum speed v_{free} , i.e., in this case $q_{\text{sat}} = q_{\text{out}}$, which is equal to 1808 vehicles/h under chosen model parameters. During the yellow phase the vehicle passes the light signal location, if the vehicle can do it until the end of the yellow phase; otherwise, the vehicle comes to a stop at the light signal.

C. Two basic moving localized patterns in three-phase theory of city traffic

As in highway traffic [17, 20, 67, 68], there are two qualitatively different localized patterns which play the basic role in theory of city traffic: a wide moving jam (Fig. 2, left panel) and a moving synchronized flow pattern (MSP) (Fig. 2, right panel). The wide moving jam satisfies the microscopic criterion for the wide moving jam phase [18, 69, 70]: there is a flow interruption interval within the jam, i.e., a long time headway(s) between vehicles (Fig. 2 (e), left panel) that is considerably longer than the mean time delay of vehicle acceleration from a standstill within the jam. During the green phase, specifically, after the queue discharge flow increases to q_{sat} , the moving queue and wide moving jam exhibit the same features; therefore, the moving queue can be considered the wide moving jam phase (J) of congested traffic in a city.

In contrast with the moving queue, there is no flow interruption within the MSP (Fig. 2 (e), right panel) – the microscopic criterion for the jam does not satisfy, i.e., the MSP belongs to the synchronized flow phase (S). To induce an MSP in free flow, a local disturbance should exceed a critical value $\Delta v_{\text{FS}}^{(\text{cr})}$ required for an F→S transition. Respectively, to induce a moving queue in free flow a local disturbance should exceed another critical value $\Delta v_{\text{FJ}}^{(\text{cr})}$ required for an F→J transition. However, at each given flow rate, at which either an F→S or F→J transition is possible, $\Delta v_{\text{FS}}^{(\text{cr})} \ll \Delta v_{\text{FJ}}^{(\text{cr})}$. This means that there is a wide range of speed disturbance amplitudes Δv_{dis} satisfying condition $\Delta v_{\text{FS}}^{(\text{cr})} \leq \Delta v_{\text{dis}} < \Delta v_{\text{FJ}}^{(\text{cr})}$ within which no moving queues can emerge, whereas MSP does occur in free flow.

D. Emergence of moving synchronized flow pattern (MSP) within green wave

At the first glance, all green waves propagate undisturbed over different cycles of the light signal (Fig. 3 (a)). However, if we consider vehicle trajectories in a larger scale (Figs. 3 (b, c)), we find that there is a small speed disturbance at the beginning of each green wave.

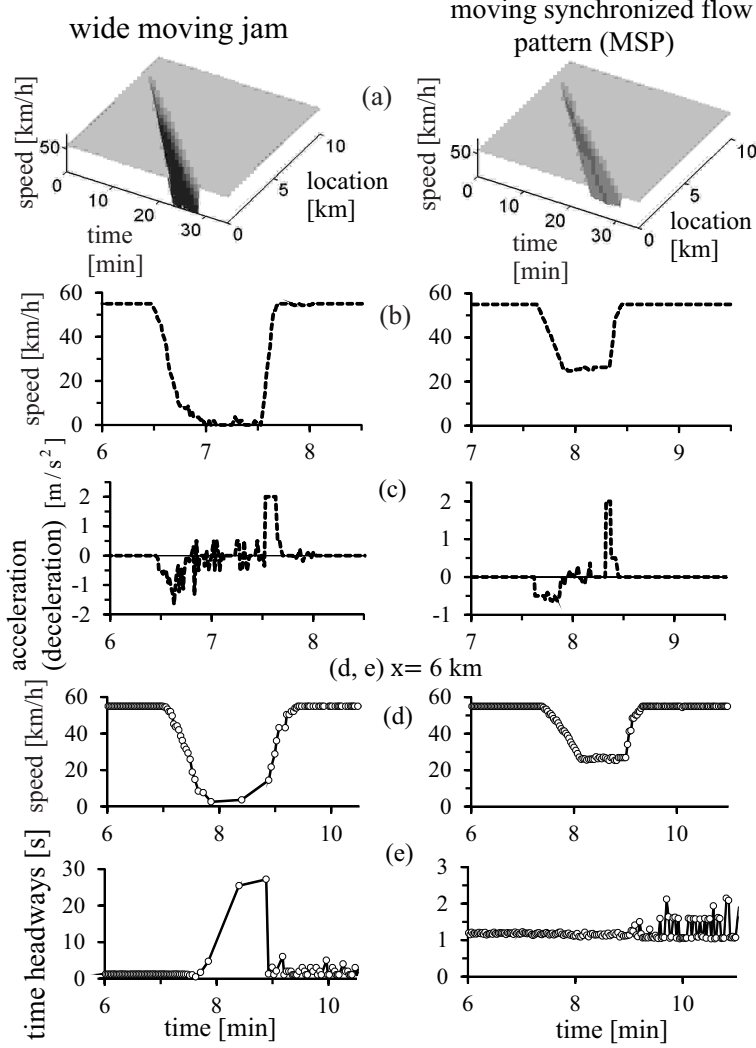


FIG. 2: Simulations of wide moving jams (left panel) and moving synchronized flow pattern (MSP) (right panel) on homogeneous single-lane road without bottlenecks: (a) Speed in time and space. (b, c) Microscopic speed (b) and acceleration (deceleration) (c) for a vehicle moving through the jam (left) or MSP (right). (d, e) Microscopic speed (d) and time headways (e) of vehicles measured at a virtual detector at location $x = 6$ km.

To understand this, we note that if a driver sees the red phase, then to stop at the light signal location $x = x_{\text{LS}}$ she/he should begin to decelerate at some distance Δx_{dis} from the light signal. When the driver is at location $x = x_{\text{LS}} - \Delta x_{\text{dis}}$ and she/he moves at the speed v_{free} , it takes the driver a time ΔT_{dis} to reach the light signal; $\Delta T_{\text{dis}} \approx 7$ s at chosen model parameters. Thus when $\Delta T_{\text{dis}} - \Delta T_{\text{b}}^{(\text{ideal})} > 0$ (Fig. 3), the driver reaching location $x = x_{\text{LS}} - \Delta x_{\text{dis}}$ decelerates during the time interval $\Delta T_{\text{dis}} - \Delta T_{\text{b}}^{(\text{ideal})}$, while seeing the red

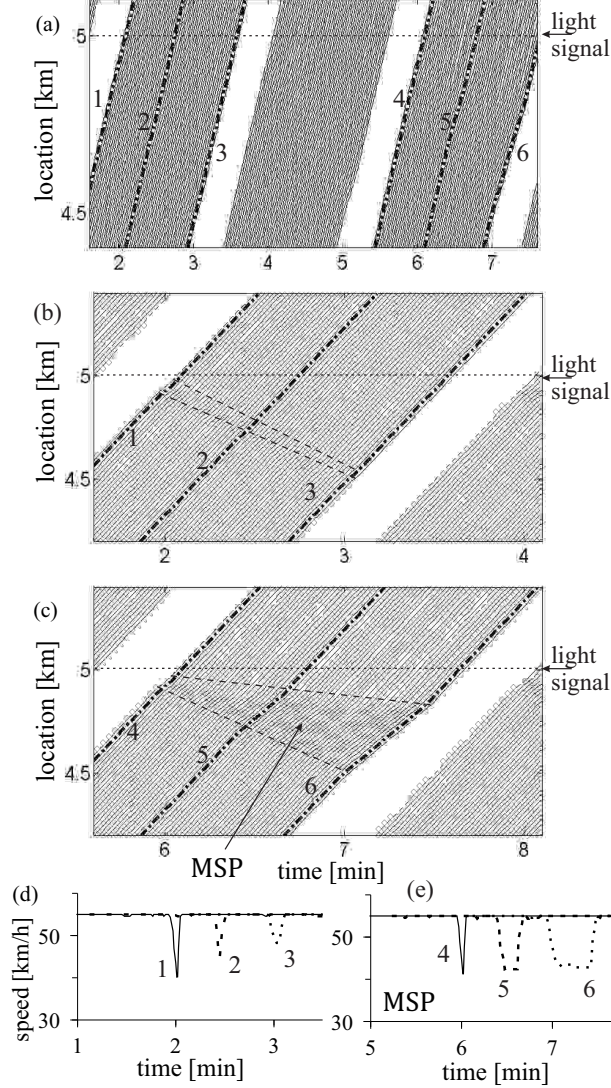


FIG. 3: Emergence of MSP within green wave at $\vartheta = 120$ s, $T_R = 20$ s, $T_Y = 2$ s, $\Delta T_b^{(\text{ideal})} = 3$ s, and $T_{\text{GW}} = 90$ s: (a–c) Vehicle trajectories within green wave. (d, e) Microscopic speeds of vehicles moving through MSPs whose numbers are related to trajectories in (a–c), respectively. In (b, c), disturbance and MSP are marked by dashed curves. $q_{\text{GW}} = 2316$ vehicles/h [71].

phase. After the green phase appears, the driver accelerates to the maximum speed v_{free} . This explains speed disturbance occurrence (curves 1 and 4 in Figs. 3 (d, e)).

In Fig. 3, we have chosen green wave parameters at which the initial disturbance amplitude is close to a critical one: In some of the light signal cycles, speed disturbances are smaller than the critical disturbance; therefore, no MSP occurs while disturbances dissolve (trajectories 1–3 in Figs. 3 (b, d)). In other cycles, speed disturbances are larger than

the critical disturbance with resulting MSP emergence (trajectories 4–6 in Figs. 3 (c, e)). Any MSP and any disturbance fully disappears at the end of each green wave and, therefore, in Fig. 3 the random process of the disturbance occurrence and development within a subsequent green wave is independent on the former green wave [72].

Through the MSP emergence time gaps ΔT_b and ΔT_e (Fig. 1) are respectively longer and shorter than $\Delta T_b^{(\text{ideal})}$ and $\Delta T_e^{(\text{ideal})}$ calculated for an undisturbed green wave (Sec. II A). Even in the same simulation realization (run) [73], parameters of MSPs that occur in different cycles are random values. Consequently, within time interval $0 < t < 34$ min the gaps ΔT_b and ΔT_e change randomly for different green waves between 3.8–4.39 s and 0.07–5.15 s, respectively; the mean values of ΔT_b and ΔT_e are respectively 3.96 s and 2.38 s (compare with $\Delta T_b^{(\text{ideal})} = 3$ s and $\Delta T_e^{(\text{ideal})} = 7$ s used in Fig. 3).

E. Common stages of green wave breakdown: Features of $\mathbf{F} \rightarrow \mathbf{S} \rightarrow \mathbf{J}$ transitions

Although an MSP emerges spontaneously in some of the light signal cycles (Figs. 3 (c, e)), no breakdown have been observed up to $t = 34$ min. However, if we consider the simulation realization shown in Fig. 3 at a longer time, we do find the phenomenon of the green wave breakdown (Figs. 4 and 5). We have found that the phenomenon of green wave breakdown begins randomly and it can be considered consisting of the following stages:

(i) *An MSP occurs and propagates upstream within the green wave* (MSP labeled by “ MSP_1 ” in Figs. 4 (a–c)).

(ii) *The last vehicle or a few of the last vehicles of the green wave come to a standstill: The random process of the green wave breakdown begins* (bold trajectory 10 in Fig. 4 (a)). The physics of stage (ii) is as follows: Vehicles exhibit delays moving through the MSP. When the delay of the last vehicle of the green wave becomes randomly longer than $\Delta T_e^{(\text{ideal})}$, the vehicle must stop at the following red phase. The random nature of this vehicle stop is associated with random characteristics of a disturbance and resulting MSP. In some other simulation realizations [73], rather than only the last vehicle of the green wave (Fig. 4 (a)), two or more vehicles must stop at the light signal.

(iii) *Synchronized flow speeds in MSPs occurring within the subsequent green waves decreases*. The vehicle(s) stopped at the light signal (item (ii)) passes it during the next green phase. This forces vehicles of the following green wave to decelerate stronger introducing a

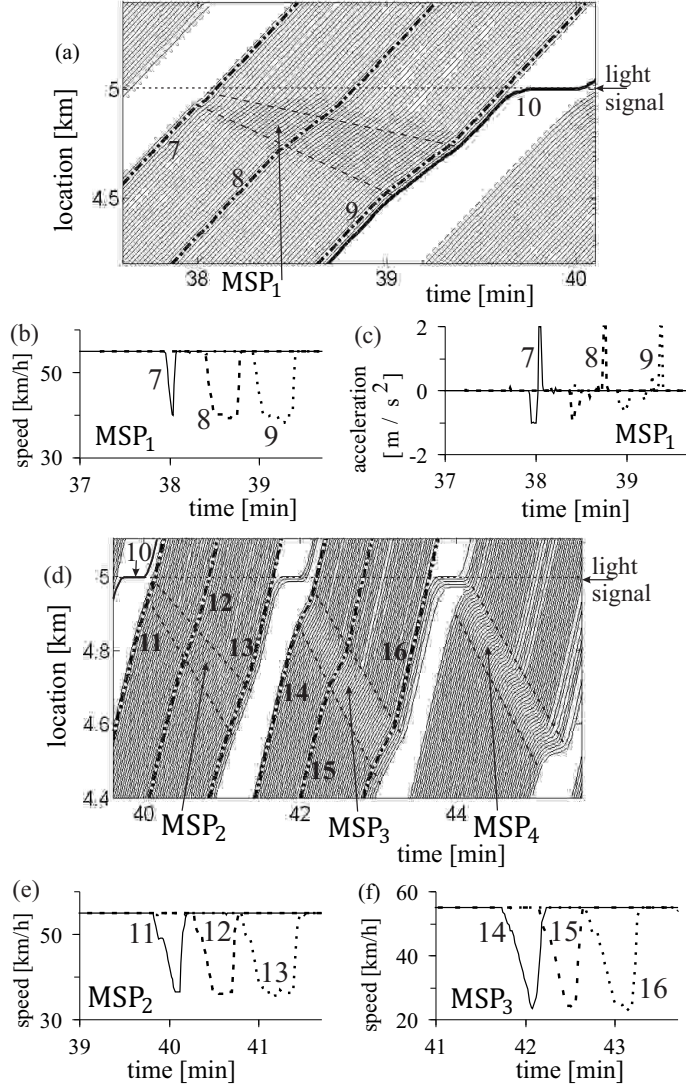


FIG. 4: Breakdown of green wave in simulation realization shown in Fig. 3: (a, d) Vehicle trajectories in different scales in which MSPs are marked by dashed curves. (b, c, e, f) Microscopic speeds (b, e, f) and acceleration (deceleration) (c) of vehicles moving thorough MSPs propagating through different green waves. Curves 7–16 in (b, c, e, f) are related to corresponding vehicle trajectories marked in (a, d).

larger disturbance within the green wave (trajectory 11 in Fig. 4 (d, e)) than in the signal cycles shown in Figs. 3 and 4 (a, b). This result is an MSP (labeled by MSP_2 in Figs. 4 (d, e)) with lower speeds (trajectories 12 and 13 in Fig. 4 (d, e)). Consequently, a larger number of vehicles at the end of the green wave exhibit a longer delay than $\Delta T_e^{(\text{ideal})}$. Therefore, more vehicles must stop at the following red phase ($t \approx 42$ min in Fig. 4 (d)). The discharge of

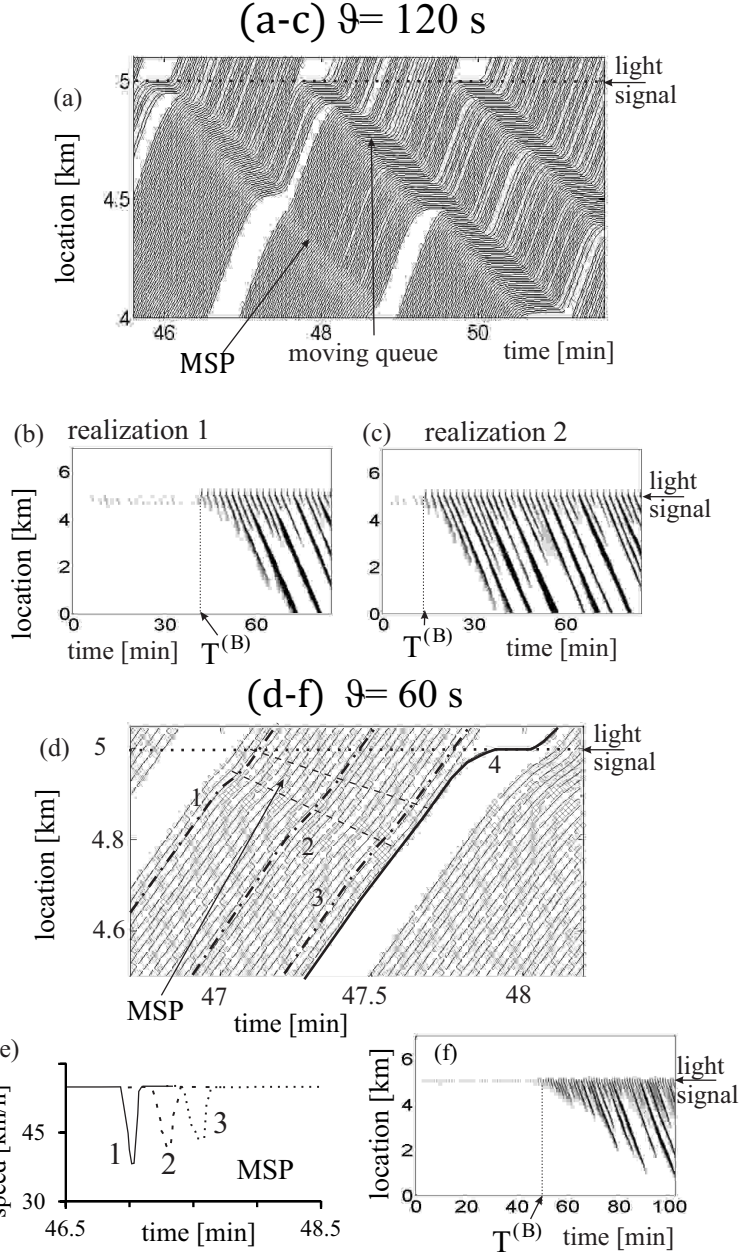


FIG. 5: Characteristics of breakdown of green waves with $\Delta T_b^{(\text{ideal})} = 3$ s for cycle times $\vartheta = 120$ s (a-c) and $\vartheta = 60$ s (d-f): (a, d) Vehicle trajectories. (b, c, f) Speed data in space-time plane presented by regions with variable shades of gray for two different realizations 1 (b) and 2 (c) [73]. (e) Microscopic speeds of vehicles 1-3 moving through MSP in (d) marked by dashed curves. In (a, b), the same realization 1 as that in Figs. 3 and 4 is used. In (a-c), model parameters are the same as those in Fig. 3. In (d-f), $\vartheta = 60$ s, $T_R = 10$ s, $T_Y = 2$ s, $T_{GW} = 45$ s, $q_{GW} = 2110$ vehicles/h [71].

this longer vehicle queue at the next green phase takes a longer time. This increases further the disturbance amplitude at the beginning of the following green wave with the further decrease in the speed within the emergent MSP (MSP_3 in Figs. 4 (d, f)). This results in the subsequent increase in the number of vehicles that must stop at the light signal: five vehicles have stopped at $t \approx 44$ min in Fig. 4 (d). The discharge of these vehicles causes MSP emergence (MSP_4 in Fig. 4 (d)) with a very low synchronized flow speed, and so on.

(iv) *The breakdown of the green wave occurs randomly with destroying of the green wave leading to the appearance of over-saturated traffic.* Stage (iii) ends abruptly at some of the cycles of the light signal: Instead of an MSP, at the beginning of the next green wave a moving queue appears that propagates through the green wave (moving queue in Fig. 5 (a)): The green wave breakdown has occurred. After the breakdown has occurred, the queue length at the light signal grows, i.e., over-saturated traffic occurs. The breakdown occurs when vehicles stopped at the beginning of the red phase forms a critical queue: When the critical queue has been reached, vehicles of the next green wave must stop approaching the end of this queue. The cycle at which the critical queue has been formed determines a time delay of the breakdown denoted by $T^{(B)}$ (Fig. 5 (b)). $T^{(B)}$ is a random value, which can change considerably in different simulation realizations [73] (Fig. 5 (b, c)).

The MSP emergence within the green wave is associated with an $F \rightarrow S$ transition. The transformation of the MSP into a moving queue (stages (iii) and (iv)) can be considered an $S \rightarrow J$ transition. Thus the green wave breakdown is associated with a sequence of $F \rightarrow S \rightarrow J$ transitions. In these $F \rightarrow S \rightarrow J$ transitions, both an $F \rightarrow S$ transition and $S \rightarrow J$ transition are random events. A time interval between random time instants of the $F \rightarrow S$ and $S \rightarrow J$ transitions can be much longer than the light signal cycle. We have found that these qualitative features of the green wave breakdown remain for a broad range of light signal parameters. This is illustrated in Fig. 5 (d–f) for $\vartheta = 60$ s.

Simulations show that when at a given q_{GW} the value $\Delta T_b^{(ideal)}$ decreases, the disturbance amplitude within the green wave increases resulting in an MSP with a low speed. In general, the larger the flow rate q_{GW} and/or the shorter the value $\Delta T_b^{(ideal)}$, the lower the speed within MSPs. At some chosen q_{GW} and $\Delta T_b^{(ideal)}$, it can turn out that rather than the MSP propagates to the end of the green wave, green wave breakdown occurs during MSP propagation through the green wave due to MSP transformation into a moving queue.

F. Green wave breakdown caused by growing speed disturbances along green wave

When at a given q_{GW} the value $\Delta T_b^{(\text{ideal})}$ increases, the disturbance amplitude at the green wave beginning decreases. Under condition

$$\Delta T_{\text{dis}} - \Delta T_b^{(\text{ideal})} \leq 0, \quad (5)$$

in contrast with green waves considered in Sec. II E no speed disturbance appears at the beginning of the green wave. However, we have revealed that even in this case the random time-delayed breakdown of the green wave can occur with probability $P^{(B)} > 0$ during a chosen time interval T_{ob} (Fig. 6).

The physics of this phenomenon is associated with many small local speed disturbances *along* the green wave. They begin to grow at different road locations along the green wave when the flow rate q_{GW} is great enough [74]. The longer the road length $x_{LS} - x_b$ (Fig. 1), the more probable that the speed disturbances become large enough before the green wave reaches the light signal; therefore, simulations show that the shorter $x_{LS} - x_b$, the larger q_{GW} at which the breakdown occurs with the same probability.

III. SELF-ORGANIZATION PHENOMENA DUE TO SPATIOTEMPORAL INTERACTION OF GREEN WAVE WITH QUEUE AT LIGHT SIGNAL

Hypothetical green waves discussed in Sec. II are a rough simplification of traffic at the light signal. In reality, there is usually turning-in traffic, which refers to traffic from the cross street that enters the lane on which the green wave travels. Turning-in traffic leads to a queue build during the red phase. The discharge of this queue can effect on the green wave considerably. We simulate turning-in traffic through flow with a rate q_{turn} occurring during the red phase; we assume that $q_{\text{turn}} < q_{GW}$ (Fig. 7 (a)).

When q_{turn} is not large (Fig. 7 (b–e)), stages (i)–(iv) of the green wave breakdown are qualitatively the same as those for $q_{\text{turn}} = 0$ (Sec. II E): The queue discharge causes a speed disturbance at the beginning of the green wave with MSP emergence (MSP_1 and MSP_2 in Fig. 7 (c, d)) (stage (i) of Sec. II E). Through vehicle delays within an MSP, after a random time interval the vehicle queue build during the red phase increases in comparison with the initial queue caused by the flow rate q_{turn} . This queue increase occurs because one or several

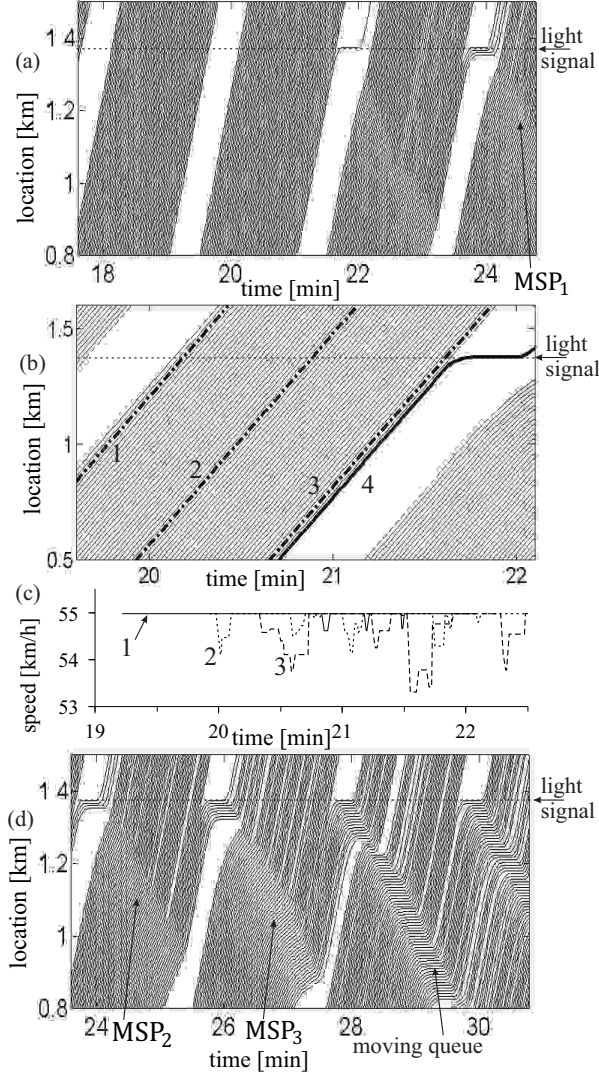


FIG. 6: Green wave breakdown under condition (5): (a, b, d) Vehicle trajectories. (c) Microscopic speeds of vehicles whose numbers related to trajectories shown in (b), respectively. $(\Delta T_b^{(\text{ideal})}, x_{\text{LS}} - x_b, q_{\text{GW}}) = (8, 1375, 2382)$ (s, m, vehicles/h) [71]. Other model parameters are the same as those in Fig. 3. For different green waves occurring within time interval $0 < t < 19$ min values ΔT_b and ΔT_e (Fig. 1) change between 7.89–8.16 s and 0.06–0.88 s, respectively.

last vehicles at the end of the green wave have to stop at the light signal (stage (ii)) (Fig. 7 (d), where the stopped vehicles of the green wave are related to bold trajectories 1 and 2, i.e., the queue increases from two vehicles associated with turning-in traffic to four vehicles). The speed within the emergent MSP decreases (MSP_3 and MSP_4 in Fig. 7 (c, e)) (stage (iii)). After a random time interval, the queue growth results in the breakdown: a moving

queue is formed (moving queue in Fig. 7 (e)) (stage (iv)).

If q_{turn} increases, then with the same probability traffic breakdown occurs at smaller flow rate q_{GW} . In general, qualitative phenomena of MSP emergence within the green wave with the subsequent random green wave breakdown remain the same as those presented above. However, when q_{turn} is large enough, the queue cannot fully dissolve before the green wave reaches the light signal (Fig. 8 (a)). When $q_{\text{GW}} < q_{\text{sat}}$ (Fig. 8), the queue dissolves during its propagation through the green wave while transforming into an MSP (dissolving moving queue and MSP_1 in Fig. 8 (a, b)). The flow rate q_{GW} in Fig. 8 is smaller than the threshold flow rate for MSP existence [17]. Therefore, the MSP begins also to dissolve during its propagation within the green wave. Nevertheless, it takes a relatively long time for this MSP dissolution: Vehicle delays become long enough for the increase in number of vehicles that stop at the light signal resulting in the breakdown (Fig. 8 (a)).

The phenomena presented in Figs. 7 and 8 remain qualitatively for any chosen difference $q_{\text{GW}} - q_{\text{turn}} > 0$ when the flow rates q_{turn} and q_{GW} are chosen on the way that probability of traffic breakdown does not change considerably ($P^{(B)} \approx 0.8$ in Figs. 7 and 8). However, the larger q_{turn} and the smaller q_{GW} , the longer the queue dissolution within the green wave and, therefore, the shorter the time interval for MSP propagation within the green wave. However, even in a limit case of a time-independent flow rate q_{in} [19] we have found MSP emergence at the end of the green phase. This MSP emergence does govern the time delayed breakdown at the light signal. One of the general results of the study made above is that a complex time-sequence of F→S→J transitions is responsible for the breakdown phenomenon at the light signal (Fig. 9).

After green wave breakdown has occurred, the resulting dynamics of over-saturated traffic upstream of the light signal exhibits complex spatiotemporal coexistence moving queues and MSPs. For example, MSPs can result from dissolving queues (MSP_2 – MSP_4 resulting from dissolving queues in Fig. 8 (c)) or an MSP can emerge at the beginning of the green wave at a relatively long distance upstream of the queue (MSP in Fig. 5 (a)).

IV. PROBABILITY OF TRAFFIC BREAKDOWN AT LIGHT SIGNAL

In each of the scenarios discussed above, traffic breakdown occurs at the light signal during the time interval $T_{\text{ob}} = 60$ min with some probability $P^{(B)} < 1$ *only* [75]. This

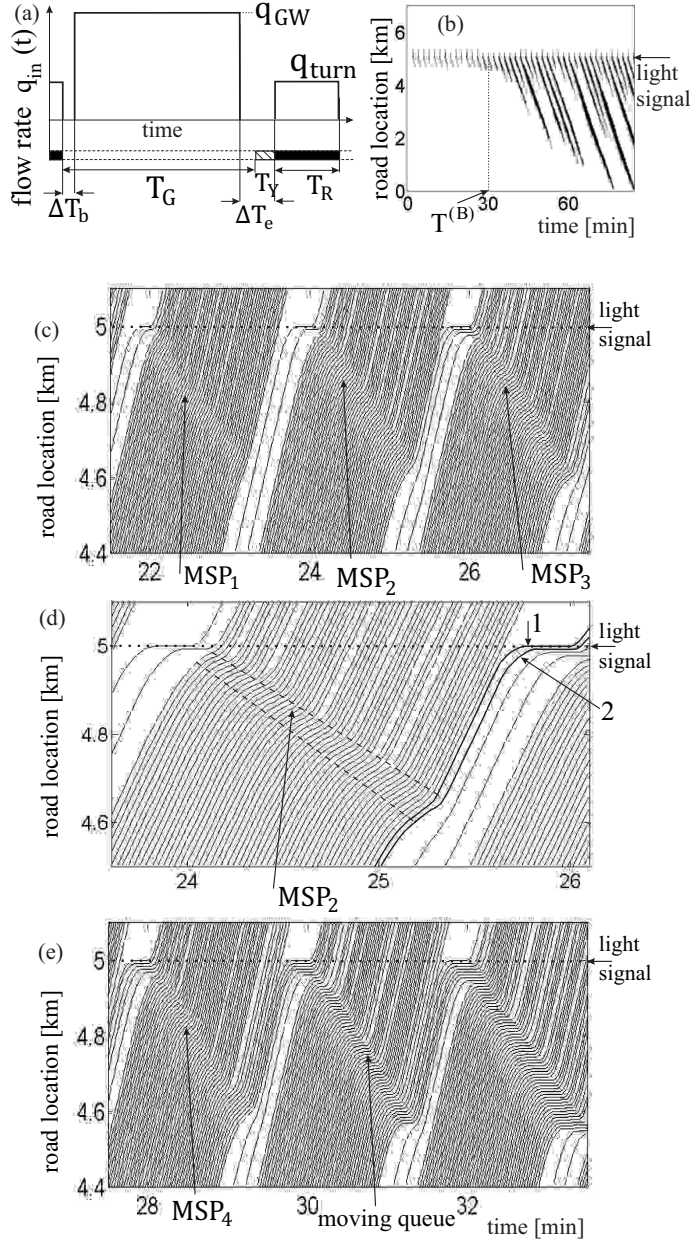


FIG. 7: Breakdown of green wave through turning-in traffic: (a) The time-dependence of the flow rate $q_{in}(t)$. (b) Speed data presented by regions with variable shades of gray. (c–e) Vehicle trajectories. $q_{GW} = 2000$ and $q_{turn} = 400$ vehicles/h. As the flow rate q_{GW} (Sec. II A), q_{turn} is determined through a given mean gross time headways τ_{turn} : $q_{turn} = 3600/\tau_{turn}$ vehicles/h. Other model parameters are the same as those in Fig. 3.

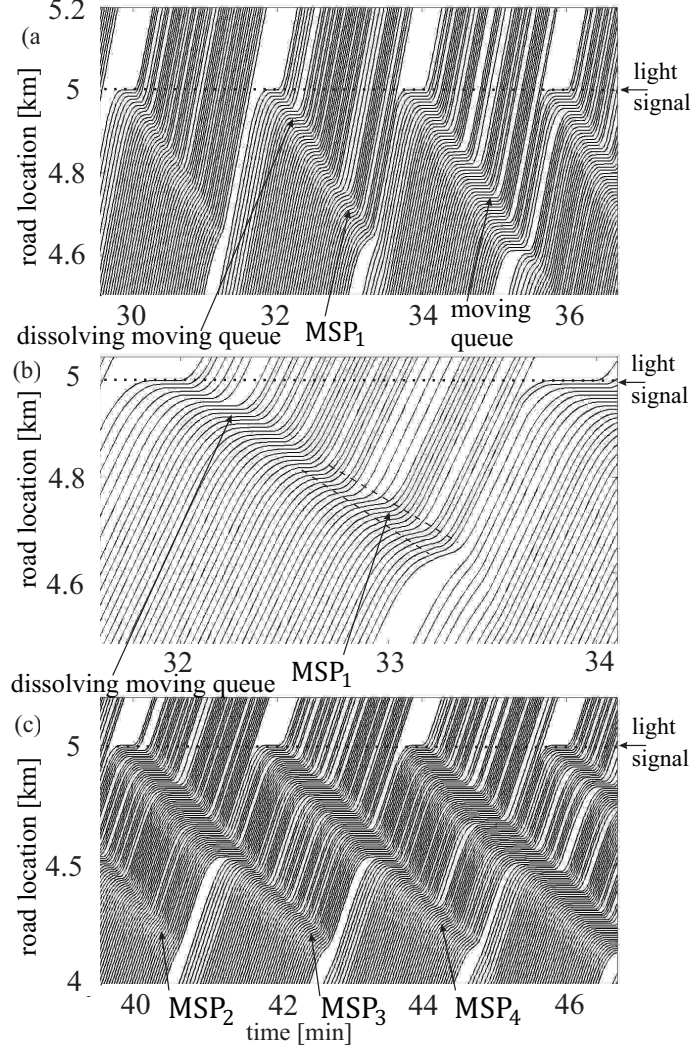


FIG. 8: Breakdown of green wave through turning-in traffic simulated with $q_{in}(t)$ shown in Fig. 7 (a): Vehicle trajectories. $q_{GW} = 1714$ and $q_{turn} = 1200$ vehicles/h. Other model parameters are the same as those in Fig. 3.

means that in some of the different numerical realizations (runs) made the breakdown does occur, however, in other realizations the breakdown does not occur [73]. We have found the following general results:

1. At given model parameters, $P^{(B)}(\bar{q}_{in})$ is an increasing function on the flow rate $\bar{q}_{in} = \vartheta^{-1} \int_0^\vartheta q_{in}(t) dt$ (Figs. 10 (a, c, e)). At a given $q_{in}(t)$, $P^{(B)}(T_R)$ is also an increasing function

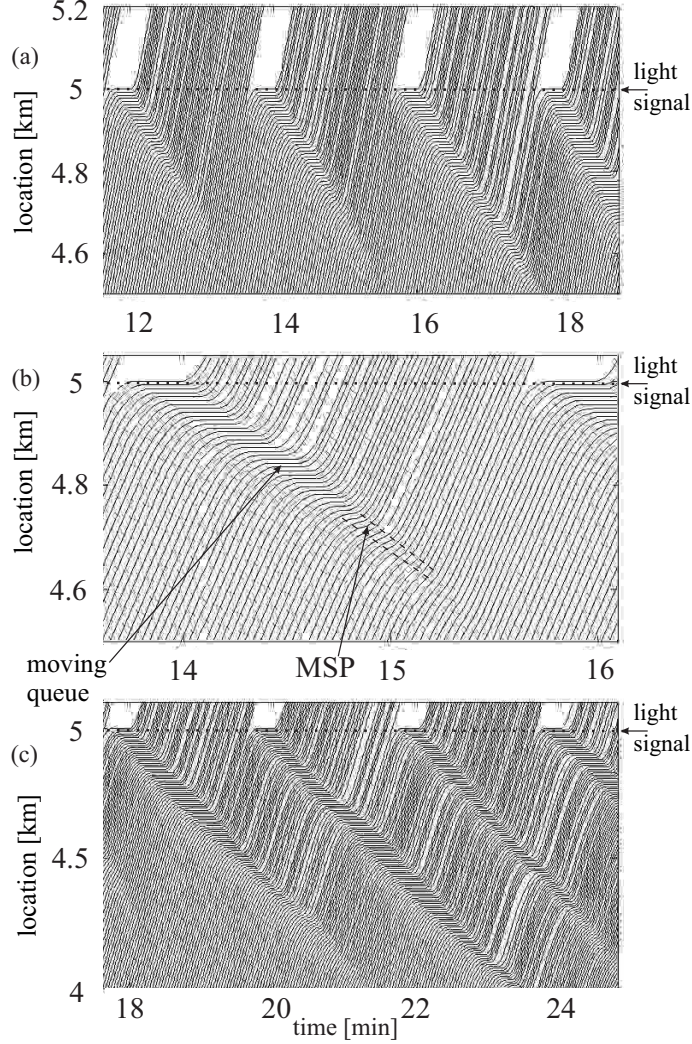


FIG. 9: Breakdown at light signal at time-independent q_{in} : Vehicle trajectories. $q_{\text{in}} = 1565$ vehicles/h. Other model parameters are the same as those in Fig. 3.

of T_{R} (Fig. 10 (b))). Functions $P^{(\text{B})}(\bar{q}_{\text{in}})$ and $P^{(\text{B})}(T_{\text{R}})$ can be fitted with

$$P^{(\text{B})}(\bar{q}_{\text{in}}) = [1 + \exp[\beta(q_{\text{p}} - \bar{q}_{\text{in}})]]^{-1}, \quad (6)$$

$$P^{(\text{B})}(T_{\text{R}}) = [1 + \exp[\beta_{\text{R}}(T_{\text{p}} - T_{\text{R}})]]^{-1}, \quad (7)$$

where β and q_{p} depend on characteristics of function $q_{\text{in}}(t)$ and light signal parameters; β_{R} and T_{p} depend on \bar{q}_{in} and ϑ .

2. When for a green wave (Fig. 1), $\Delta T_{\text{b}}^{(\text{ideal})}$ increases from 0 to 8 s, function $P^{(\text{B})}(\bar{q}_{\text{in}})$ moves to larger values \bar{q}_{in} (curves 1–4 in Fig. 10 (c)): The longer $\Delta T_{\text{b}}^{(\text{ideal})}$, the smaller the speed disturbance at the begin of the green wave. This results in shorter vehicle delays.

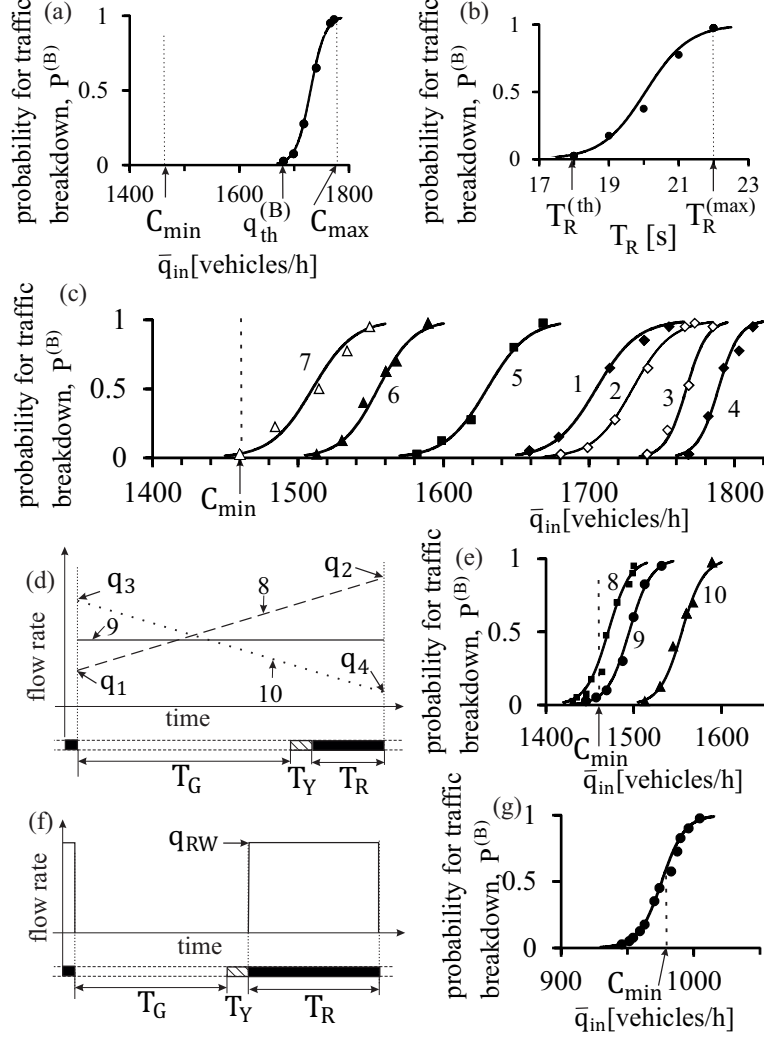


FIG. 10: Probability of breakdown at light signal: (a, b) Breakdown probability $P^{(B)}$ for $\Delta T_b^{(\text{ideal})} = 3$ s as a function of average flow rate \bar{q}_{in} (a) at $T_R = 20$ s and as a function of T_R at $q_{\text{GW}} = 2316$ vehicles/h (b). (c) Comparison of functions $P^{(B)}(\bar{q}_{\text{in}})$ for $\Delta T_b^{(\text{ideal})} = 0$ (curve 1), 3 s (curve 2), 6 s (curve 3), 8 s (curve 4 at $x_{\text{LS}} = 1375$ m [71]), 10 s (curve 5) as well as turning-in traffic (Sec. III) associated with the change in q_{turn} (curves 6 and 7 related to q_{GW} given in Figs. 7 and 8, respectively). (d, e) Functions $P^{(B)}(\bar{q}_{\text{in}})$ (e) for different time-dependences $q_{\text{in}}(t)$ (d) shown by the same numbers in (d) and (e); in (d), $q_1 = 0.35q_2$, $q_4 = 0.35q_3$. (f, g) “Red wave” of duration T_R (f) and related function $P^{(B)}(\bar{q}_{\text{in}})$ (g). $T_R = 10$ (a, c, e) and 52 s (g). Other model parameters are the same as those in Fig. 3. $C_{\text{min}} = 1461$ in (a, c, e) and 979 vehicles/h in (g) (see Sec. V).

However, this effect has a limit: At a given T_{GW} , the increase in $\Delta T_{\text{b}}^{(\text{ideal})}$ leads to a decrease in $\Delta T_{\text{e}}^{(\text{ideal})}$. Therefore, already a relatively short vehicle delays can cause the stop of a vehicle(s) from the end of the green wave at the light signal. This explains why the whole function $P^{(\text{B})}(\bar{q}_{\text{in}})$ begins to move back to smaller flow rates \bar{q}_{in} (curve 5 in Fig. 10 (c)). This shift of $P^{(\text{B})}(\bar{q}_{\text{in}})$ to the smaller \bar{q}_{in} increases when turning-in traffic occurs: The smaller the relation $q_{\text{GW}}/q_{\text{turn}}$, the larger the shift (curves 6 and 7 in Fig. 10 (c)).

3. In general, the shift of $P^{(\text{B})}(\bar{q}_{\text{in}})$ to the smaller \bar{q}_{in} is the more, the longer the queue build during the previous red phase. This effect is shown in Fig. 10 (d, e) for three different periodic functions $q_{\text{in}}(t) = q_{\text{in}}(t + \vartheta)$ associated with an increase in $q_{\text{in}}(t)$ over time (curve 8), time-independent flow rate (curve 9), and a decrease in $q_{\text{in}}(t)$ (curve 10). We have found that the larger the relation $q_{\text{in}}^{(\text{green})}/q_{\text{in}}^{(\text{red})}$, the more the shift of the function $P^{(\text{B})}(\bar{q}_{\text{in}})$ to larger \bar{q}_{in} (Fig. 10 (e)), where $q_{\text{in}}^{(\text{red})} = T_{\text{R}}^{-1} \int_{\vartheta - T_{\text{R}}}^{\vartheta} q_{\text{in}}(t) dt$ and $q_{\text{in}}^{(\text{green})} = (\vartheta - T_{\text{R}})^{-1} \int_0^{\vartheta - T_{\text{R}}} q_{\text{in}}(t) dt$.

V. INFINITE NUMBER OF CAPACITIES OF LIGHT SIGNAL

Traffic capacity of the light signal C is defined as the average flow rate downstream of the light signal \bar{q}_{LS} at which traffic breakdown can occur.

For each set of a given time-dependence of arrival flow rate $q_{\text{in}}(t)$ and light signal parameters there are the infinite number of such capacities, which are within the range

$$C_{\text{min}} \leq C \leq C_{\text{max}}, \quad (8)$$

where C_{min} is the classical capacity, i.e., $C_{\text{min}} = C_{\text{cl}}(1)$, which we call the minimum capacity, and C_{max} is the maximum capacity associated with the occurrence of spontaneous breakdown at the light signal.

We define spontaneous breakdown as a random time-delayed transition from under- to over-saturated traffic. All examples presented above are related to spontaneous breakdown. For each given time-dependence $q_{\text{in}}(t)$ and given light signal parameters, spontaneous breakdown occurs with probability $P^{(\text{B})}(\bar{q}_{\text{in}}) > 0$ during the time interval T_{ob} within a range of \bar{q}_{in} (Fig. 10 (a))

$$q_{\text{th}}^{(\text{B})} \leq \bar{q}_{\text{in}} \leq C_{\text{max}}, \quad (9)$$

where $q_{\text{th}}^{(\text{B})}$ is a threshold flow rate for spontaneous breakdown: at $\bar{q}_{\text{in}} < q_{\text{th}}^{(\text{B})}$ breakdown probability $P^{(\text{B})}(\bar{q}_{\text{in}}) = 0$. The maximum capacity C_{max} is defined as the average flow rate \bar{q}_{in}

at which breakdown probability $P^{(B)}$ reach 1 during the time interval $T_{ob} : P^{(B)}|_{\bar{q}_{in}=C_{max}} = 1$. The sense of maximum capacity is as follows: Under conditions $q_{th}^{(B)} \leq \bar{q}_{in} < C_{max}$, spontaneous breakdown can occur during the time interval T_{ob} , however, with probability $P^{(B)} < 1$. This means that in some of realizations [73] no breakdown occurs; therefore, the *maximum* capacity is not still reached. Contrarily, when $\bar{q}_{in} = C_{max}$, then during the time interval T_{ob} spontaneous breakdown does definitely occur.

VI. INDUCED TRAFFIC BREAKDOWN AND DOUBLE Z-CHARACTERISTIC

The minimum capacity C_{min} can be considerably smaller than $q_{th}^{(B)}$ (Fig. 11 (a)). However, under condition $\bar{q}_{in} < q_{th}^{(B)}$ probability of spontaneous breakdown is equal to zero. Nevertheless, in accordance with (8) within the flow rate range

$$C_{min} \leq \bar{q}_{in} < q_{th}^{(B)} \quad (10)$$

under-saturated traffic is in a metastable state with respect to the transition to over-saturated traffic. Therefore, in this flow rate range the breakdown can be induced by external time-limited disturbances in under-saturated traffic. Induced breakdown can occur even if a disturbance appears during *only one* of the light signal cycles. Examples of such disturbances are a random deceleration of one of the vehicles within a green wave or a queue caused by turning-in traffic.

For a green wave (Fig. 1), we choose the flow rate $\bar{q}_{in} = q_{GW}(T_{GW}/\theta)$ satisfying condition (10) (Fig. 12). Then $P^{(B)} = 0$, i.e., no green wave breakdown can occur spontaneously. Now, during the red phase of *the only one cycle* M_{turn} vehicles appear due to turning-in traffic ($M_{turn} = 7$ at $t \approx 15.7$ min in Fig. 12 (a)). The vehicles are build a queue during the red phase. The discharge of the queue at the following green phase causes a speed disturbance occurring within the associated green wave. We have found the following phenomena: (i) For each given \bar{q}_{in} that satisfies (10) there is a value of M_{turn} at which the disturbance induces breakdown with some probability during the time interval T_{ob} [76]. The smaller \bar{q}_{in} , the larger M_{turn} is required for the breakdown (Fig. 12 (c)). (ii) The speed disturbance causes the emergence of an MSP within the green wave. (iii) The subsequent development of the MSP, which is qualitatively the same as that for spontaneous breakdown (Sec. II E), leads

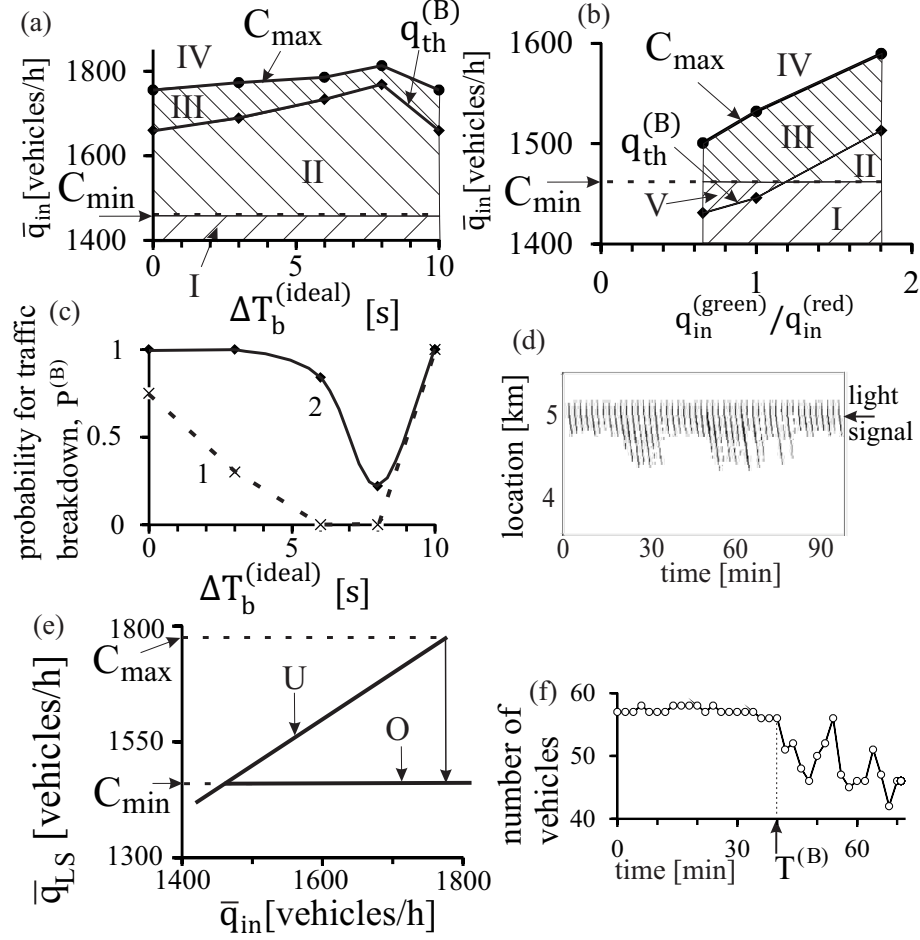


FIG. 11: Characteristics of the infinite number of capacities at light signal: (a, b) Diagrams of breakdown for green wave associated with functions $P^{(B)}(\bar{q}_{in})$ shown by curves 1–5 in Fig. 10 (c) and curves 8–10 in Fig. 10 (e), respectively, for (a) and (b). (c) Probability of spontaneous breakdown as function of $\Delta T_b^{(ideal)}$ for two given flow rates $\bar{q}_{in} = 1720$ (dashed curve 1) and 1780 vehicles/h (solid curve 2) associated with (a). (d) Speed data in the space-time plane of for dissolving over-saturated traffic occurring within region V in diagram (b) for function $q_{in}(t)$ shown by curve 8 in Fig. 10 (d) for $\bar{q}_{in} - C_{min} = -15$ vehicles/h, $q_1 = 746$ and $q_2 = 2130$ vehicles/h. (e, f) Flow–flow characteristics $\bar{q}_{LS}(\bar{q}_{in})$ (e) and dependence of number of vehicles passing the light signal (f) for green waves with $\Delta T_b^{(ideal)} = 3$ s related to Fig. 3.

to over-saturated traffic.

A sequence of $F \rightarrow S \rightarrow J$ transitions at the light signal (Secs. II and III) can be presented in the speed–flow-rate plane by a double Z-characteristic for phase transition in traffic at

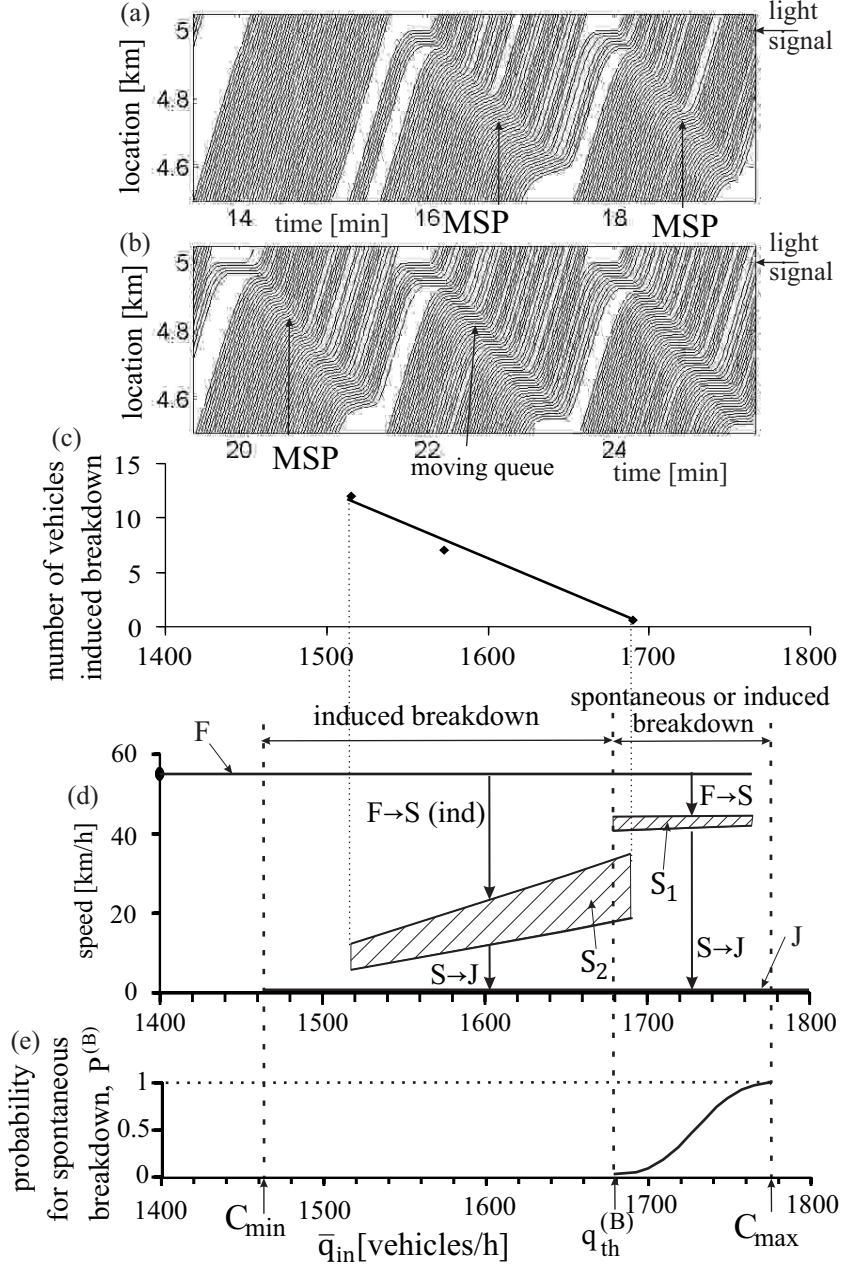


FIG. 12: Induced traffic breakdown at light signal: (a, b) Vehicle trajectories for $q_{GW} = 2057$ vehicles/h and $M_{\text{turn}} = 7$ vehicles. (c) Number of vehicles M_{turn} inducing breakdown as function of \bar{q}_{in} . $(q_{\text{th}}^{(B)}, C_{\text{max}}) = (1680, 1772)$ vehicles/h. (d) Double Z-characteristic. (e) Breakdown probability taken from Fig. 10 (a). In (d), regions S_1 and S_2 are related to synchronized flow within MSPs. Other parameters the same as those in Fig. 3.

the light signal (Fig. 12 (d)), which exhibits the following characteristics: (i) An F→S transition with MSP emergence shown by arrow “F→S”. (ii) An S→J transition shown by arrow “S→J” [81]. (iii) Under condition (9), spontaneous F→S→J transitions can occur with probability $P^{(B)}(\bar{q}_{in}) > 0$ during the time interval T_{ob} (Fig. 12 (e)). (iv) Under condition (10), an F→S transition (labeled by “F→S (ind)”) can be induced. (v) Under condition (9), regions of induced and spontaneous breakdowns are partially overlapping each other: the breakdown can be induced before spontaneous breakdown occurs.

VII. DIAGRAM OF TRAFFIC BREAKDOWN AT LIGHT SIGNAL

A diagram of the breakdown presents regions of the flow rate \bar{q}_{in} , within which the breakdown can occur, in dependence of light signal parameters or/and parameters of the time-function $q_{in}(t)$ (Fig. 11 (a, b)). Regions I–V in the diagrams (Fig. 11 (a, b)) have the following meaning: I is related to stable under-saturated traffic, II – metastable under-saturated traffic, III – metastable under-saturated traffic in which spontaneous breakdown can occur, IV – unstable under-saturated traffic, and in region V *dissolving* over-saturated traffic can occur. In dissolving over-saturated traffic, random emergence and subsequent dissolution of a growing queue at the light signal follows each other randomly (Fig. 11 (d)).

The maximum capacity C_{max} , which determines top diagram boundary, can exhibit a maximum as a function of light signal parameters (Fig. 11 (a)). An analysis of this diagram shows that there is a minimum of breakdown probability $P^{(B)}$ as a function of $\Delta T_b^{(ideal)}$ at given other parameters (Fig. 11 (c)).

A. “Red” wave: Transition to classical definition of capacity at light signal

The smaller the relation $q_{in}^{(green)}/q_{in}^{(red)}$, the smaller the difference $C_{max} - C_{min}$ (Fig. 11 (b)). In the limit case $q_{in}^{(green)}/q_{in}^{(red)} = 0$, which we call “red” wave because all vehicles arrive the light signal during the red phase only (Fig. 10 (f)), the difference $C_{max} - C_{min}$ becomes very small. Therefore, the transition from under- to over-saturated traffic occurs on average at $\bar{q}_{in} = C_{min}$ as stated in the classical traffic flow theories [1, 15, 16, 77]. Thus only for the red wave one can determine traffic capacity at the light signal based on the classical capacity definition (Sec. I). This emphasizes that and why in all realistic cases in which during the

green and yellow phases $q_{\text{in}}(t) \neq 0$ there are the infinite number of capacities at the light signal within the capacity range (8).

B. Flow–flow characteristic of green wave breakdown

A flow–flow characteristic explains the evolution of green wave in the flow–flow plane with coordinates $(\bar{q}_{\text{LS}}, \bar{q}_{\text{in}})$, where $\bar{q}_{\text{LS}} = \vartheta^{-1} \int_0^{\vartheta} q_{\text{LS}}(t) dt$ is average rate in the light signal outflow, i.e., downstream of the light signal (Figs. 1 and 11 (e)): If \bar{q}_{in} (Sec. II A) increases beginning from small values, $\bar{q}_{\text{LS}} = \bar{q}_{\text{in}}$ (branch *U* for under-saturated traffic in Fig. 11 (e)). Under-saturated traffic associated with green wave can exist even when $\bar{q}_{\text{in}} > C_{\text{min}}$. However, at $\bar{q}_{\text{in}} = C_{\text{max}}$ during the time interval T_{ob} with probability $P^{(\text{B})} = 1$ the green wave breakdown does occur: The green wave destroys resulting in the decrease in the outflow rate from $\bar{q}_{\text{LS}} = C_{\text{max}}$ to $\bar{q}_{\text{LS}} = C_{\text{min}}$ (arrow from branch *U* to branch *O* for over-saturated traffic) caused by the breakdown. Before green wave breakdown occurs, the number of vehicles passing the light signal is almost time-independent ($t < T^{(\text{B})}$ in Fig. 11 (f)); after the breakdown it exhibits a very complex time behavior ($t > T^{(\text{B})}$).

After over-saturated traffic has occurred, the presented theory shows the well-known result of the classical theory [1, 15, 16]: When over-saturated traffic exists at the light signal (branch *O* in Fig. 11 (e)), a large decrease in \bar{q}_{in} to $\bar{q}_{\text{in}} < C_{\text{min}}$ is needed for the return transition to under-saturated traffic.

VIII. BREAKDOWN OF GREEN WAVE AT SEQUENCE OF LIGHT SIGNALS

We consider green wave propagation through a sequence of the light signals at equidistant locations $x = x_{\text{LS}}^{(p)}$ with a distance between them Δx_{LS} and a time shift of the green phase beginning $\Delta T_{\text{G}} = \Delta x_{\text{LS}}/v_{\text{free}}$, where $p = 1, 2, 3, \dots, P$; $P > 1$ is the number of the light signals. We have revealed the following results (Figs. 13–16): (i) In a neighborhood of *each* of the light signals an MSP can occur. Because vehicles move through MSPs occurring at different light signals, the mean values of random time gaps ΔT_{b} and ΔT_{e} depend on the light signal location (see caption to Fig. 15). (ii) Stages of the green wave breakdown are the same as those found for the isolated light signal (Sec. II E). (iii) However, there is a stochastic *dynamic competition* in the development of the green wave breakdown *between*

light signals. In particular, it turns often out that although a queue appears firstly at one of the light signals (stage (ii) of Sec. II E), the breakdown is realized (stage (iv) of Sec. II E) at another one. Characteristic features of this dynamics depend on values $\Delta T_b^{(\text{ideal})}$ and Δx_{LS} (Figs. 13–16):

1. If Δx_{LS} is considerably shorter than the distance that an MSP propagates to the green wave end (about 400 m in Fig. 3), then with the largest probability the breakdown occurs at one of the upstream light signals. In Fig. 13, vehicles within the green wave should propagate through an MSP occurring at the upstream light signal that they approach (MSP_2 in Fig. 13 (c, d)) and through another MSP occurring at the subsequent downstream light signal (MSP_1). Both MSPs merge within the green wave into one MSP with a larger width (MSP_Σ in Fig. 13 (c, d)). This increases vehicle delays within the MSPs resulting in the breakdown at the upstream light signal.

2. Under condition (5) no MSPs appear initially at the beginning of green waves (Sec. II F). Although at a short value Δx_{LS} with the largest probability the breakdown occurs also at one of the upstream light signals (Fig. 14 (b, d)), in different realizations [73] the stop of a vehicle(s) initiating the breakdown process is observed at different light signals (trajectories 1 and 2 in Fig. 14 (a) and (c), respectively).

3. If Δx_{LS} is long enough, then with the largest probability the breakdown occurs at one of the downstream light signals (Fig. 15 (a, b)): Approaching the furthest downstream light signal vehicles exhibit the longest mean time delay caused by MSPs within the green wave.

4. When Δx_{LS} is comparable with the distance that the MSP propagates to the green wave end, the stop of last vehicles of the green wave (stage (ii) of Sec. II E) can occur at several neighborhood light signals. In example shown in Fig. 16, the stop of the last vehicle of a green wave occurs at the downstream light signal (trajectories 1 in Fig. 16 (a)). This results in MSPs emerging at the downstream light signal. One of the MSPs (MSP marked in Fig. 16 (b)) can cause the vehicle stop at the neighborhood upstream light signal (trajectory 2 in Fig. 16 (b)). In turn, this vehicle stop decreases the number of vehicles within the green wave approaching the downstream light signal. This results in the interruption of the breakdown process at this light signal: The breakdown process that has started at the downstream light signal leads to the breakdown at one or a few of the upstream light signals (Fig. 16 (c, d)).

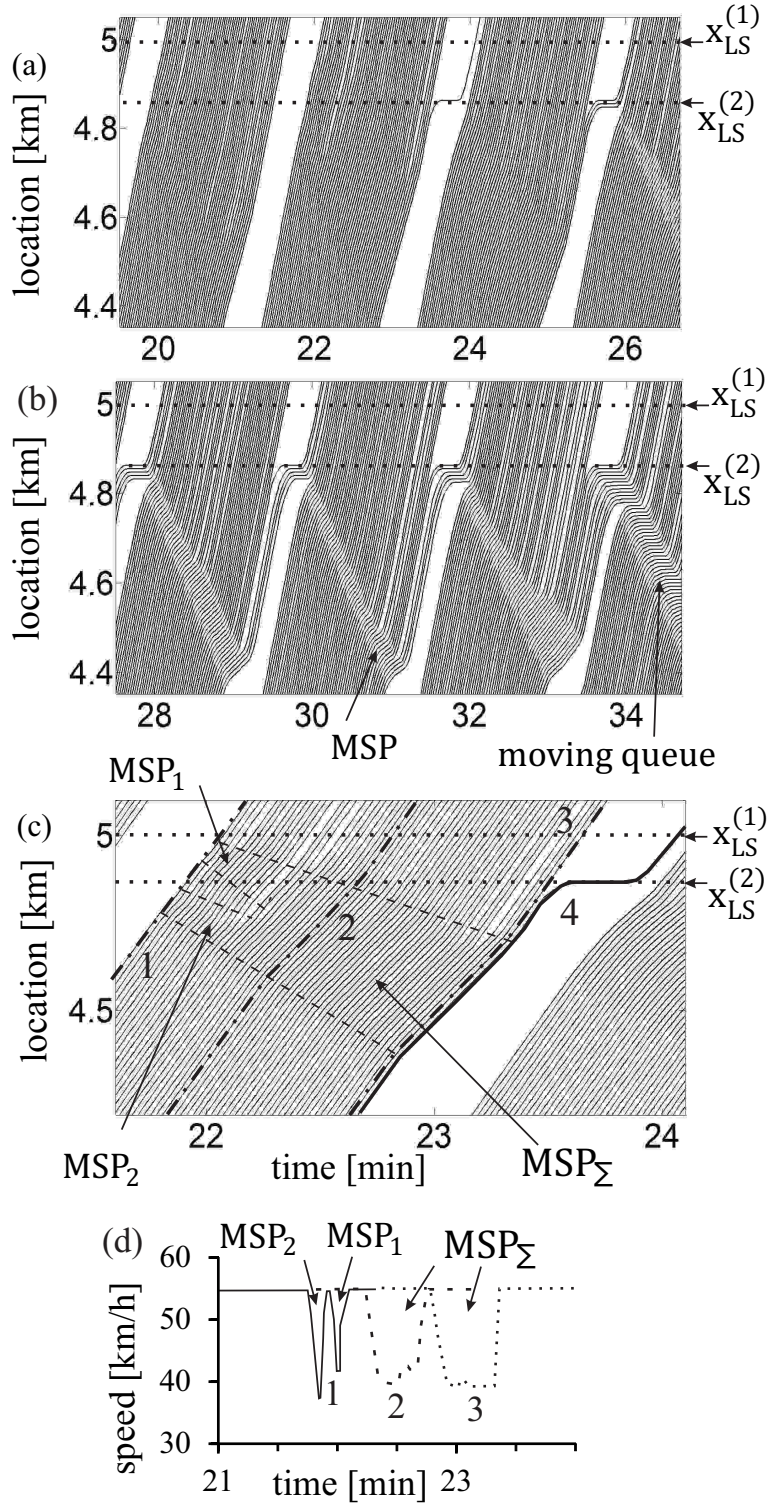


FIG. 13: Green wave breakdown at two light signals at $\vartheta = 120$ s, $T_R = 20$ s, $T_{GW} = 90$ s, and $\Delta T_b^{(\text{ideal})} = 3$ s: (a-c) Vehicle trajectories. (d) Microscopic speeds of vehicles moving through MSPs labeled in (c). $\Delta x_{LS} = 137.5$ m [71]. $q_{GW} = 2292$ vehicles/h.

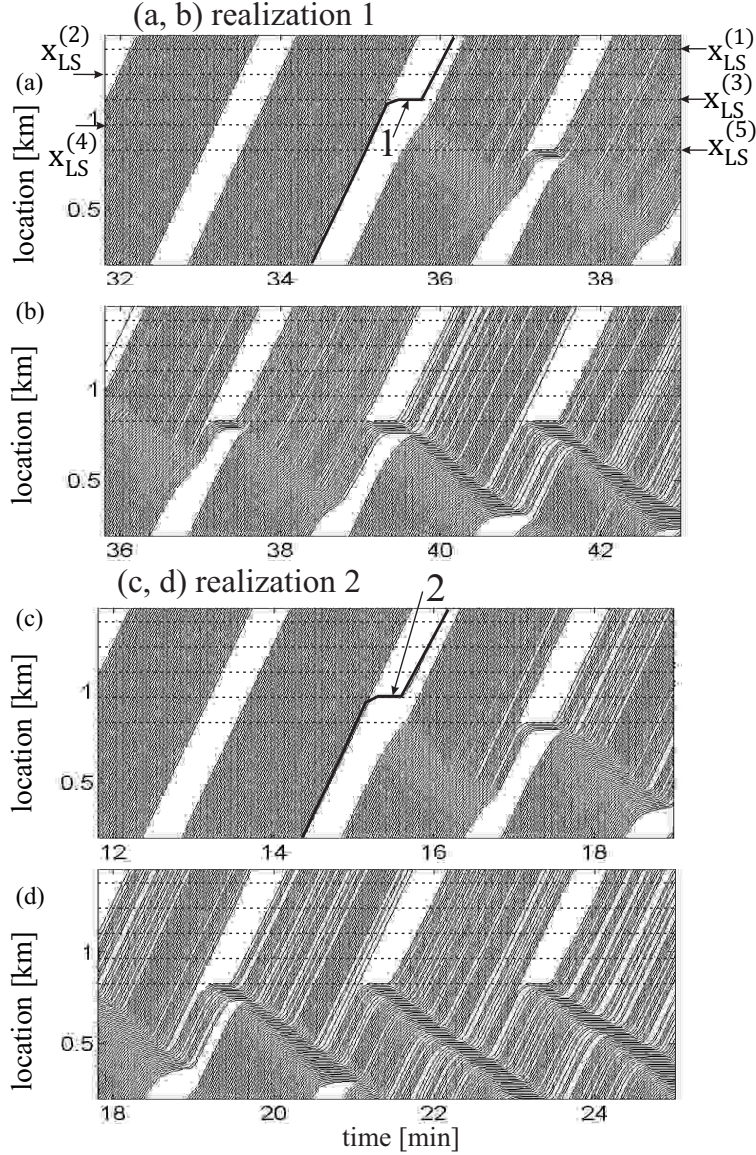


FIG. 14: Green wave breakdown at five light signals at $\vartheta = 120$ s, $T_R = 20$ s, $T_{GW} = 90$ s, and $\Delta T_b^{(\text{ideal})} = 8$ s: Vehicle trajectories for realization 1 (a, b) and 2 (c, d). $\Delta x_{LS} = 137.5$ m, $x_{LS}^{(1)} - x_b = 1375$ m [71]. $q_{GW} = 2382$ vehicles/h.

IX. APPLICATIONS OF BREAKDOWN MINIMIZATION (BM) PRINCIPLE FOR OPTIMIZATION OF GREEN WAVE IN A CITY

For a traffic network with N bottlenecks the BM principle is as follows [78–80]: The network optimum is reached, when dynamic traffic optimization and/or control are performed in the network in such a way that the probability for spontaneous occurrence of traffic break-

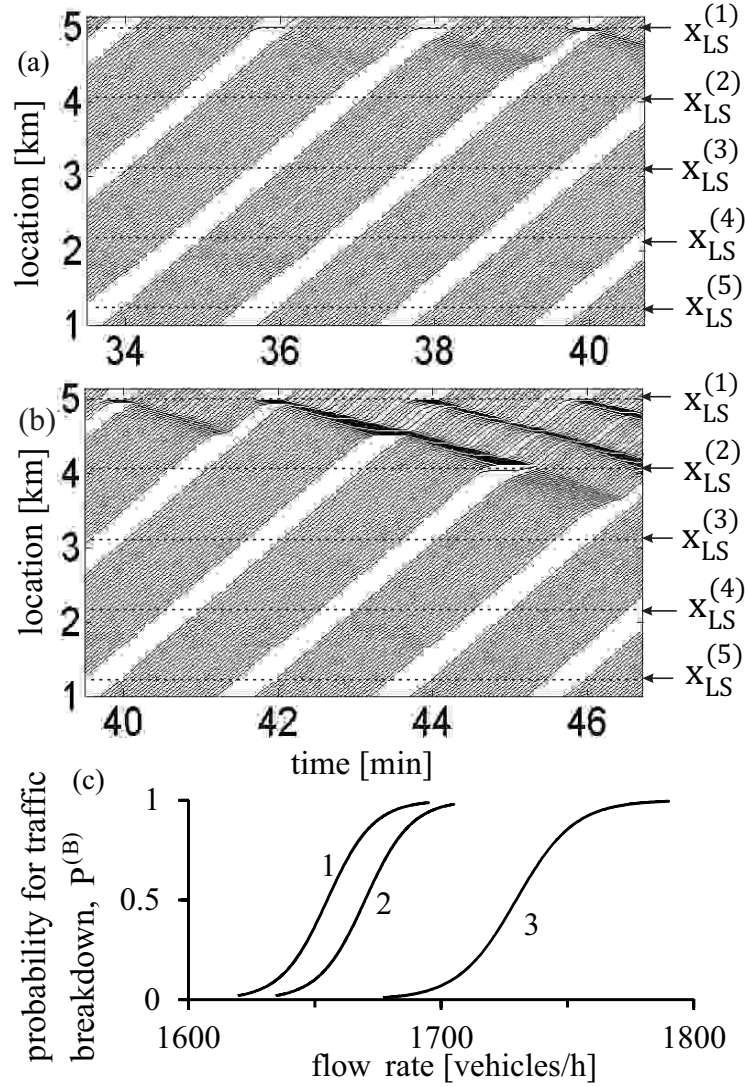


FIG. 15: Green wave breakdown at five light signals at $\vartheta = 120$ s, $T_R = 20$ s, $T_{GW} = 90$ s, and $\Delta T_b^{(\text{ideal})} = 3$ s: (a, b) Vehicle trajectories; $\Delta x_{LS} = 962.5$ m [71]. (c) Functions $P^{(B)}(\bar{q}_{in})$ of probability that green wave breakdown occurs at *one of the light signals* during the time interval T_{ob} (curves 1 and 2 for $\Delta x_{LS} = 687.5$ and 137.5 m, respectively) and their comparison with $P^{(B)}(\bar{q}_{in})$ for isolated light signal (curve 3 taken from Fig. 10 (a)). In (a, b), within time interval $0 < t < 34$ min for different green waves we find the following ranges of random changes in time gaps $(\Delta T_b^{(p)}, \Delta T_e^{(p)}) = (5.32\text{--}5.93, 0.05\text{--}3.41)$, $(5.11\text{--}5.71, 0.28\text{--}3.9)$, $(4.8\text{--}5.4, 0.81\text{--}4.99)$, $(4.4\text{--}4.8, 0.87\text{--}5.3)$, and $(3.79\text{--}4.43, 2.77\text{--}6.78)$ s for $p = 1, 2, \dots, 5$, respectively; the mean values of these time gaps are $(5.61, 1.99)$, $(5.3, 2.33)$, $(5.01, 2.95)$, $(4.56, 3.87)$, and $(3.95, 5.13)$ s for $p = 1, 2, \dots, 5$, respectively. $q_{GW} = 2252$ vehicles/h.

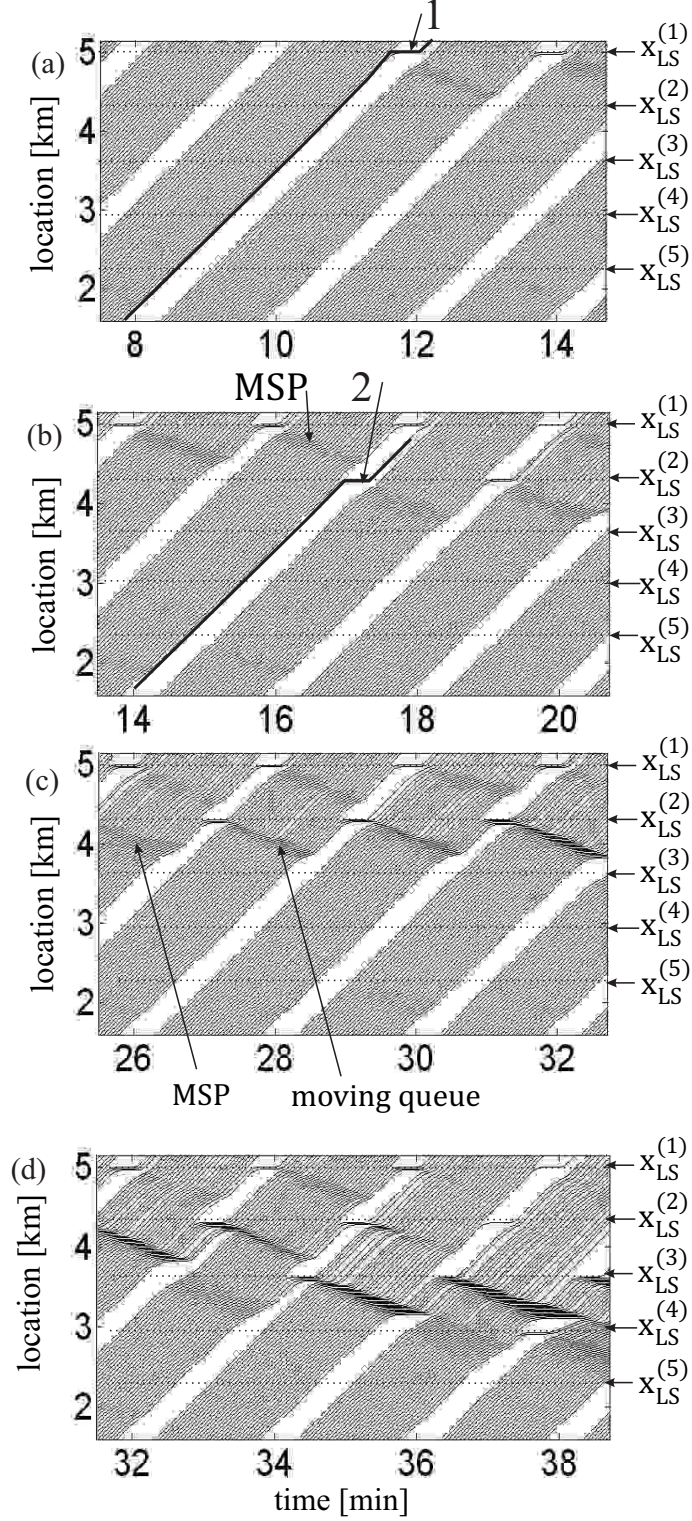


FIG. 16: Green wave breakdown at five light signals at $\vartheta = 120$ s, $T_R = 20$ s, $T_{GW} = 90$ s, and $\Delta T_b^{(\text{ideal})} = 3$ s: Vehicle trajectories. $\Delta x_{LS} = 687.5$ m [71]. $q_{GW} = 2252$ vehicles/h.

down in at least one of the network bottlenecks during a given observation time T_{ob} reaches the minimum possible value. The BM principle is equivalent to the maximization of the probability that traffic breakdown occurs at *none* of the network bottlenecks.

Assuming that traffic breakdown at different bottlenecks in the network is independent each other, the probability for spontaneous occurrence of traffic breakdown in at least one of the network bottlenecks during the time interval T_{ob} can be written as:

$$P_{\text{net}} = 1 - \prod_{k=1}^N (1 - P^{(\text{B},k)}). \quad (11)$$

In accordance with the BM principle, the network optimum is reached at [78–80]

$$\min_{q_1, q_2, \dots, q_M, \zeta_1, \zeta_2, \dots, \zeta_M, \alpha_1, \alpha_2, \dots, \alpha_W} \{P_{\text{net}}(q_1, q_2, \dots, q_M, \zeta_1, \zeta_2, \dots, \zeta_M, \alpha_1, \alpha_2, \dots, \alpha_W)\}, \quad (12)$$

where M is the number of network links for which inflow rates can be adjusted, q_m is the link inflow rate for a link with index m ; ζ_m is a matrix of percentages of vehicles with different vehicle (and/or driver) characteristics that influence on the breakdown probability at a bottleneck; the matrix ζ_m takes into account that dynamic assignment is possible individually for each of the vehicles [82]; $m = 1, 2, \dots, M$, where $M > 1$; $k = 1, 2, \dots, N$ is bottleneck index, $N > 1$; $P^{(\text{B},k)}$ is probability that during the time T_{ob} traffic breakdown occurs at bottleneck k ; α_w is the set of control parameters for one of these N bottlenecks with index w ($w = 1, 2, \dots, W$), $W \leq N$ [83]. The BM principle is equivalent to

$$\max_{q_1, q_2, \dots, q_M, \zeta_1, \zeta_2, \dots, \zeta_M, \alpha_1, \alpha_2, \dots, \alpha_W} \{P_{\text{C},\text{net}}(q_1, q_2, \dots, q_M, \zeta_1, \zeta_2, \dots, \zeta_M, \alpha_1, \alpha_2, \dots, \alpha_W)\}, \quad (13)$$

where

$$P_{\text{C},\text{net}} = \prod_{k=1}^N P_{\text{C}}^{(\text{B},k)} \quad (14)$$

is the probability that during time interval T_{ob} free flows remain in the network, i.e., that traffic breakdown occurs at *none* of the bottlenecks,

$$P_{\text{C}}^{(\text{B},k)} = 1 - P^{(\text{B},k)}. \quad (15)$$

The existence of a minimum of breakdown probability on the time gap $\Delta T_{\text{b}}^{(\text{ideal})}$ (Fig. 11 (c)) allows us to suggest some simple applications of the BM principle for the green wave optimization. In a hypothetical case of a sequence of light signals $k = 1, \dots, N_1$ that are at long enough distances each other the green wave optimization at given θ , T_{R} , T_{G} , and T_{GW}

can be achieved by a choice of optimal values $\Delta T_{b,k}^{(\text{ideal})}$, $k = 1, \dots, N_1$. Indeed, in the case the BM principle (12) leads to a simple result that the optimum for green wave is reached, when each of the breakdown probabilities $P^{(B,k)}$ for the associated light signals $k = 1, \dots, N_1$ reaches minimum as a function of $\Delta T_{b,k}^{(\text{ideal})}$.

In the case of a complex dynamic competition between the light signals $k = 1, \dots, N_1$ (Sec. VIII), traffic breakdowns at these different light signals cannot be considered independent events. However, these light signals we can consider a *single bottleneck*. In the BM principle (11), (12), breakdown probability $P^{(B,s)}$ for this single bottleneck with some index $k = s$ is associated with probability for the breakdown occurring at *one* of the light signals during the time interval T_{ob} . Simulations show that for a sequence of the light signals the function $P^{(B)}(\bar{q}_{\text{in}})$ satisfies formula (6) and it is usually shifted to smaller flow rates in comparison with the function $P^{(B)}(\bar{q}_{\text{in}})$ for an isolated light signal (Fig. 15 (c)). This application of the BM principle is possible only when $N_1 < N$, i.e., when in addition to the single bottleneck caused by the light signals there are also other bottlenecks in the network.

As introduced in [78–80], traffic network optimization through the use of the BM principle can be a combination of a *global* network optimization with *local* control of a bottleneck consisting of the following stages:

(i) *Global network optimization*: The minimization of traffic breakdown probability in the network based on the BM principle.

(ii) *Local bottleneck control*: A spatial limitation of congestion growth when traffic breakdown has nevertheless occurred at a network bottleneck, with the subsequent congestion dissolution at the bottleneck, if the dissolution of congestion due to traffic management in a neighborhood of the bottleneck is possible.

(iii) *Combination of global network optimization with local control of congested bottlenecks*: The minimization of traffic breakdown probability with the BM principle in the network part that is not influenced by congestion together with local control of congested bottlenecks mentioned in item (ii).

We see that in the approach of traffic network optimization and control of Ref. [78–80], local bottleneck control begins only after the process of traffic breakdown has already started at the bottleneck and, therefore, this network bottleneck cannot further be included in global network optimization with the BM principle (12).

Local bottleneck control can be very effective for a green wave because between the start

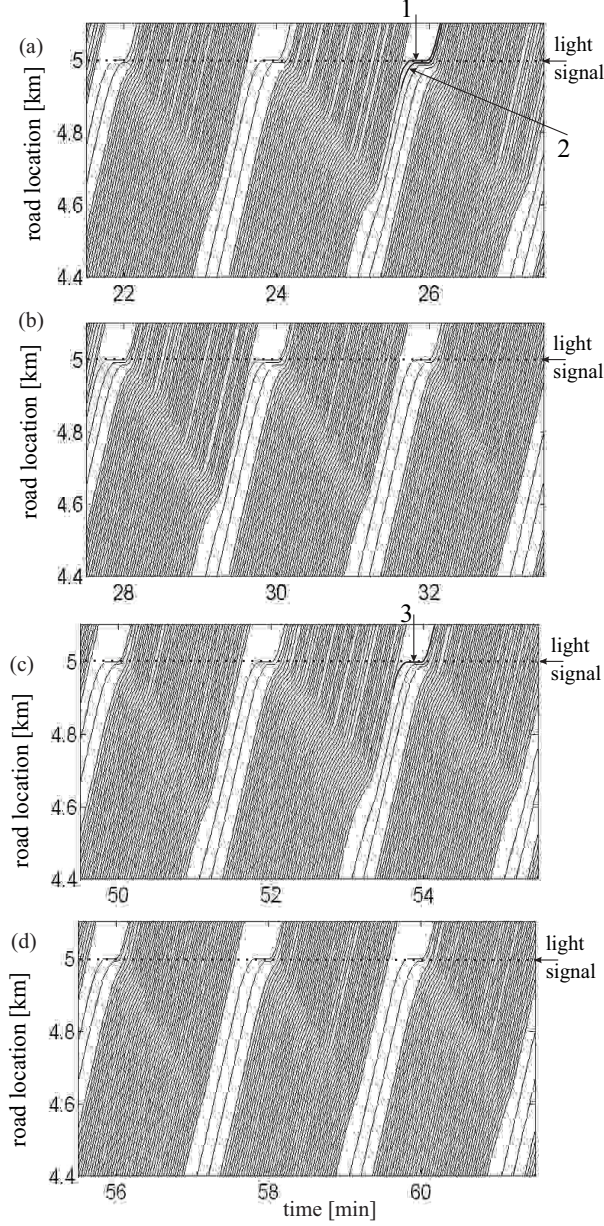


FIG. 17: Control of green wave breakdown shown in Fig. 7. Vehicle trajectories: (a, b) Interruption of breakdown process due to control. After two last vehicles of green wave come to a stop at $t \approx 25.8$ min (bold trajectories 1 and 2 are the same as 1 and 2 in Fig. 7 (d)), T_R is set to be 1 s shorter for the *only* one light signal cycle. In (b), due to control the number of stopped vehicles decreases at the next cycle (from two vehicles to one vehicle) although for subsequent cycles T_R remains to be 20 s. (c, d) Green wave control shown in (a, b) repeats each time, when the breakdown process starts over time (in (c) the last vehicle of the green wave comes to a stop at $t \approx 53.8$ min as shown by bold trajectory 3); as in (a, b), this control results in breakdown interruption (d).

of the breakdown (stage (ii) of Sec. II E) and the breakdown instant (stage (iv) of Sec. II E) there can be a long time interval associated with several cycles of the light signal. Through appropriate control made within this time interval the breakdown process can be interrupted as shown in Fig. 17.

After congestion dissolution or breakdown interruption has been achieved at the bottleneck, this bottleneck can again be included in global network optimization with the BM principle (12). If rather than congestion dissolution or breakdown interruption at the bottleneck (Fig. 17) only the limitation of the congestion growth can be achieved through traffic management in a neighborhood of a bottleneck, global network optimization with the BM principle is performed only for a network part that is not influenced by congestion: In (11), breakdown probabilities for only those network bottlenecks at which no congestion has occurred should be taken into account.

X. DISCUSSION

A. Comparison of traffic breakdown at highway bottleneck and light signal

$F \rightarrow S \rightarrow J$ transitions disclosed above as the reason for traffic breakdown at the light signal occur because remaining vehicles stopping at the previous red cycle act as a disturbance for the next traffic. A large enough on-ramp inflow at an on-ramp bottleneck acts also as disturbance for traffic on the main road causing $F \rightarrow S \rightarrow J$ transitions at the highway bottleneck [17, 23]. Therefore, questions arise: What new features are induced by the existence of traffic lights in comparison with those for the on-ramp bottleneck? Is the effect of vehicles stopping at the previous red cycle of the light signal different from those of in-coming traffic at on-ramp? Responses to these questions are as follows.

1. During the red phase, traffic is interrupted at the light signal resulting in a vehicle queue. The downstream queue front is fixed at the light signal: The outflow from this queue *is zero*. In contrast, during the whole time and independent on on-ramp inflow the outflow from congested traffic at the on-ramp bottleneck *is not zero*. This leads to the following qualitative different traffic features at the light signal and on-ramp bottleneck:

- (i) Due to the $F \rightarrow S$ transition, a widening SP (WSP) or localized SP (LSP) (SP – synchronized flow pattern) can occur at the on-ramp bottleneck [17]. The downstream

front of the WSP or LSP is fixed at the bottleneck. Within this front vehicles accelerate from synchronized flow upstream of the on-ramp bottleneck to free flow downstream. The existence of the WSP or LSP is possible because the on-ramp bottleneck does not interrupt traffic flow. In contrast, the light signal interrupts traffic flow during the red phase. For this reason, neither WSP nor LSP can occur at the light signal.

(ii) Rather than WSP or LSP emergence, the $F \rightarrow S$ transition occurring in arrival traffic during the green phase leads to an MSP whose downstream front propagates upstream of the light signal.

(iii) During the green phase, the downstream front of the queue moves upstream as those for a wide moving jam in highway traffic. Therefore, this moving queue is a synonym of the wide moving jam. However, the moving queue occurs at the light signal. In contrast, wide moving jams emerge at some distance from the on-ramp bottleneck location at which the $F \rightarrow S$ transition has initially occurred [17, 84].

2. Traffic breakdown at the on-ramp bottleneck is an $F \rightarrow S$ transition: After the $F \rightarrow S$ transition has occurred, synchronized flow (one of the phases of congested traffic) remains at the bottleneck. In contrast, traffic breakdown at the light signal is associated with $F \rightarrow S \rightarrow J$ transitions. This is because an $F \rightarrow S$ transition in arrival traffic at the light signal leads to MSP emergence that does not necessarily cause the breakdown at the light signal. When MSP emergence leads to the breakdown, there can be a long time-sequence of many $F \rightarrow S$ transitions with MSP formation in each of the subsequent light signal cycles before the breakdown (transition from under- to over-saturated traffic) occurs. These traffic phenomena that are characteristic ones for the light signal do not occur at the on-ramp bottleneck.

B. Comparison of traffic breakdown at light signal within the frameworks of three-phase and two-phase traffic flow theories

A two-phase model follows from the three-phase model (Sec. IIB) after removing the description of driver behaviors associated with three-phase theory [17, 18] – 2D-region of synchronized flow states (dashed region S in Fig. 1 (b)) as well as a competition between the speed adaptation and over-acceleration effects have been removed; this is done through the use of $G_n = 0$ and $p_a = p_1 = p_2 = 0$ in the three-phase model (Appendix C). As a result, steady states of the two-phase model are related to a fundamental diagram (Fig. 1

(c)). In the two-phase model traffic breakdown is governed by a phase transition from free flow to the jam (F→J transition) [85]. All characteristics of a wide moving jam in the three-phase and two-phase models are *identical*, in particular, the flow rate in free flow in the jam outflow is equal to $q_{\text{out}} = q_{\text{sat}} = 1808$ vehicles/h. Both models exhibit the same and well-known traffic behavior at light signal [15]: (i) at small flow rates \bar{q}_{in} a vehicle queue dissolves fully during the green phase (under-saturated traffic), and (ii) at great enough \bar{q}_{in} the queue grows non-reversibly (over-saturated traffic) leading to traffic gridlock [19].

Nevertheless, we have found that at the same flow rate $\bar{q}_{\text{in}} = q_{\text{GW}}(T_{\text{GW}}/\vartheta)$ and other model parameters as those used in simulations with three-phase model shown in Fig. 4 in *none* of simulation realizations made with two-phase model the green wave breakdown can occur (Fig. 18 (a)). To understand this, note that at any given flow rate \bar{q}_{in} probability of a sequence of F→S→J transitions occurring in three-phase model (curve labeled by F→S in Fig. 18 (b)) is considerably larger than probability of an F→J transition that occurs in two-phase model (curve labeled by F→J in Fig. 18 (b)). For this reason, although in two-phase model simulations there are also initial speed disturbances at the beginning of the green waves (Fig. 18 (c)), however, *no* MSPs have emerged through these disturbances. This is because in contrast with in three-phase model, there is no synchronized flow in two-phase model. As a result, in two-phase model the amplitude of the initial disturbances decreases during their propagation through the green waves (Fig. 18 (d)).

The result that at any given flow rate probability of an F→S transition is considerably greater than that of an F→J transition (Fig. 18 (b)) is a general one: This is also valid for a highway bottleneck as shown in Fig. 18 (g).

Thus the green wave breakdown in two-phase model occurs at considerably larger flow rates \bar{q}_{in} than those in three-phase model. At these large flow rates, the initial disturbance with a considerably lower speed occurs causing long vehicle delays. The subsequent breakdown development is qualitatively similar to that found with three-phase models explained above (Figs. 18 (e, f)).

The result that at a given flow rate \bar{q}_{in} probability of a sequence of F→S→J transitions (three-phase model) is considerably larger than probability of an F→J transition (two-phase model) remains also when \bar{q}_{in} is smaller than the threshold flow rate for the MSP existence q_{th} in three-phase model (Sec. II C). This is explained in Fig. 19 through a consideration of the dissolution of a wide moving jam on a homogeneous road without light signals and other

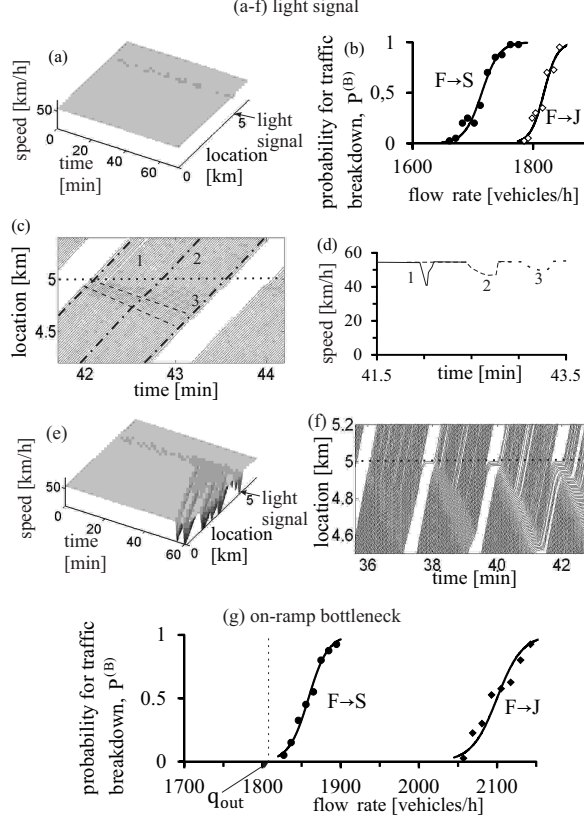


FIG. 18: Comparison of three-phase and two-phase models for simulations of traffic at light signal (a–f) and at on-ramp bottleneck (g): (a) Speed in space and time simulated with two-phase model at the same model parameters as those in Fig. 4. (b) Probability of breakdowns of green wave as functions of \bar{q}_{in} with three-phase model (curve labeled by $F \rightarrow S$) and with two-phase model (curve labeled by $F \rightarrow J$). (c, d) Vehicle trajectories (c) and associated microscopic speeds along vehicle trajectories 1–3 (d) related to (c). (e, f) Speed in space and time and trajectories for green wave breakdown simulated with two-phase model at greater \bar{q}_{in} than that in (a, c, d). (g) Probability for traffic breakdown at on-ramp bottleneck in three-phase model (curve $F \rightarrow S$) and in two-phase model (curve $F \rightarrow J$). In (a, c–f), $q_{GW} = 2316$ (a, c, d) and 2446 vehicles/h (e, f). Other parameters in (a–f) are the same as those in Fig. 3. In (g), $q_{on} = 300$ vehicles/h.

bottlenecks. In three-phase model, after the jam has dissolved a dissolving MSP occurs, which dissolves slowly (figures in left panel in Fig. 19 (c, e)). This causes a much slower dissolution of a local region of lower speed than this occurs in two-phase model (right panel in Fig. 19 (c, e)) in which no synchronized flow can appear.

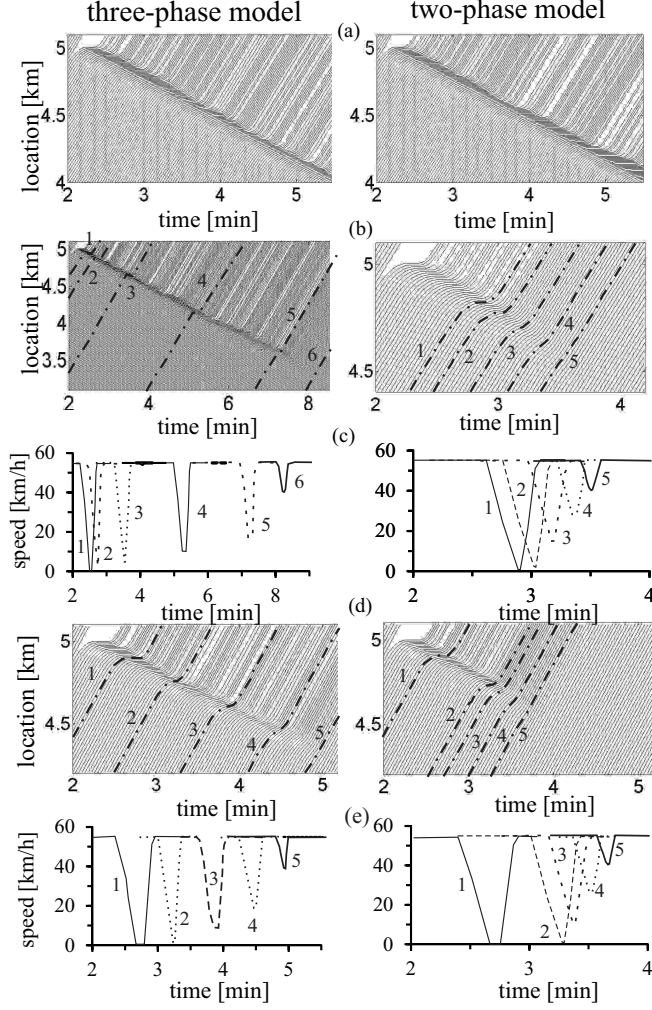


FIG. 19: Features of dissolution of wide moving jam (queue dissolution) in three-phase model (left panel) and two-phase model (right panel): (a, b, d) Vehicle trajectories for wide moving jam propagation without jam dissolution at $q_{in} = q_{out}$ (a) and under jam dissolution occurring at $q_{in} < q_{out}$ (b, d). (c, e) Vehicle speed along trajectories related to (b, d), respectively. Simulations on traffic flow on homogeneous road without light signal and other bottlenecks. To induced initial wide moving jam, one of the vehicles comes to a stop for 10 s; after this the vehicle accelerates in accordance with model rules of vehicle motion. $q_{in} = 1808$ (a), 1800 (b, c) 1565 vehicles/h (d, e).

C. Conclusions

1. There are very complex spatiotemporal self-organized traffic phenomena, which govern traffic behavior in city traffic, in particular, traffic capacity at the light signal.
2. The delayed spontaneous breakdown of a green wave is initiated by the emergence of

an MSP within the green wave. The MSP causes delays for vehicles that can randomly lead to a stop of one (or several) vehicle(s) moving at the end of the green wave. The discharge of a queue of the stopped vehicles causes an MSP with a lower synchronized flow speed, and so on. Long vehicle delays within an MSP result in a long queue build during the red phase. For one of the subsequent green waves, this queue cannot dissolve before arrival of the following green wave. This causes traffic breakdown, i.e., the transition from under- to over-saturated traffic at the light signal.

3. There are the infinite number of capacities of traffic at the light signal, which are in a capacity range between a minimum capacity and maximum capacity. Each of the capacities within the capacity range gives the flow rate at which the breakdown can occur.

4. The minimum capacity is equal to the capacity of the classical theory (Sec. I). The maximum capacity determines the flow rate at which the random time-delayed breakdown occurs spontaneously during a given time interval with probability that is equal to 1.

5. Within the capacity range, two capacity regions separated by a threshold flow rate can be distinguished. In the first capacity region (between minimum capacity and threshold flow rate), an induced sequence of $F \rightarrow S \rightarrow J$ transitions, i.e., the induced breakdown can occur only. In the second capacity region (between threshold flow rate and maximum capacity), a time-delayed spontaneous breakdown occurs during a given time interval.

6. At a given average arrival flow rate, both the maximum capacity and threshold flow rate depend crucially on a time-dependence of this flow rate: The larger the number of vehicles that arrive the light signal during the green phase of the light signal, the larger the maximum capacity and the larger the threshold flow rate.

7. For time-functions of the flow rate studied, the largest maximum capacity and threshold flow rate are possible for a hypothetical green wave in which all vehicles arrive the light signal during the green phase only, i.e., when there is no an initial vehicle queue at the light signal.

8. The $F \rightarrow S \rightarrow J$ transitions and infinite number of capacities of traffic at the light signal can be well presented by a double Z-speed-flow-rate characteristic.

9. Probability of green wave breakdown as a function of light signal parameters can have a minimum in some flow rate range. This can be used for green wave optimization with the BM principle.

10. Green wave breakdown at a sequence of the light signals exhibits a complex spa-

tiotemporal dynamics of the breakdown process associated with MSPs occurring upstream of different light signals.

For a test of these and other conclusions, an empirical study of speed disturbances and MSP emergence within a green wave should be made. To solve this problem, measurements of *single vehicle speed along the whole green wave* are required that (for the author knowledge) are not currently available. Such measurements and their analysis will be an interesting task for a future study of the physics of traffic in a city. For engineering applications, an additional theoretical analysis of speed disturbances and MSP emergence within the green wave caused by left or right turns and the width of the intersection can be important.

Acknowledgments:

I thank German research and development project “UR:BAN” for support. I thank Sergey Klenov and Viktor Friesen for discussions and Sergey Klenov for help in simulations.

Appendix A: Definitions and symbols

In under-saturated traffic at the light signal, all vehicles, which are waiting within a queue during the red phase, can pass the signal during the green phase. An opposite case occurs in over-saturated traffic and, therefore, the queue grows.

Traffic breakdown at the light signal is the transition from under- to over-saturated traffic. Spontaneous breakdown is a random time-delayed breakdown.

Traffic capacity of the light signal C is the average flow rate downstream of the light signal \bar{q}_{LS} at which traffic breakdown can occur at the light signal.

Turning-in traffic refers to traffic from the cross street that enters the lane on which the green wave travels.

F – free flow, S – synchronized flow, J – a moving queue at the light signal. An F→S transition is a local phase transition from free flow to synchronized flow occurring in arrival flow at the light signal. The F→S transition leads to the emergence of a moving synchronized flow pattern (MSP). A sequence of F→S→J transitions means the MSP emergence (F→S transition) with the subsequent emergence of a moving queue (S→J transition) resulting in the breakdown at the light signal.

q_{sat} is the saturation flow rate, i.e., the mean flow rate from a queue at the light signal during the green phase when vehicles discharge to the maximum free speed v_{free} ($q_{sat} = 1808$

vehicles/h under chosen model parameters).

$\vartheta = T_G + T_Y + T_R$ is the cycle time of the light signal. T_G , T_Y , and T_R are durations of the green, yellow, and red phases of the light signal, respectively.

x_b and x_{LS} are coordinates of the road beginning and isolated light signal, respectively. In a light signal sequence, Δx_{LS} is a distance between the light signals that are at locations $x_{LS}^{(p)}$, $p = 1, 2, \dots, P$, where P is the number of the light signals.

T_{GW} and q_{GW} are respectively the green wave duration and flow rate within green wave given at location $x = x_b$.

ΔT_b is a random time gap between the end of the red phase and beginning of the green wave. ΔT_e is a random time gap between the end of green wave and beginning of the red phase. $\Delta T_b^{(\text{ideal})}$ and $\Delta T_e^{(\text{ideal})}$ are respectively values of ΔT_b and ΔT_e under hypothetical vehicle motion at the speed v_{free} .

$T^{(B)}$ is a random time delay of traffic breakdown at the light signal.

T_{ob} is a time interval for observing traffic (in all simulations $T_{\text{ob}} = 60$ min).

$P^{(B)}$ is breakdown probability during the time interval T_{ob} .

$q_{\text{in}}(t)$ is the rate of arrival traffic at the light signal that average value is $\bar{q}_{\text{in}} = \vartheta^{-1} \int_0^{\vartheta} q_{\text{in}}(t) dt$.

q_{turn} is the flow rate in turning-in traffic.

q_{LS} is the rate of flow downstream of light signal (in the light signal outflow) that average value is $\bar{q}_{LS} = \vartheta^{-1} \int_0^{\vartheta} q_{LS}(t) dt$.

C_{min} and C_{max} are respectively the minimum and maximum traffic capacities at the light signal.

$\bar{q}_{\text{in}} = q_{\text{th}}^{(B)}$ is a threshold flow rate for spontaneous breakdown.

Variables and values of a stochastic microscopic traffic flow model used in simulations are explained in Appendix B.

Appendix B: Kerner-Klenov three-phase microscopic traffic flow model for signal-lane road

Rules of vehicle motion in three-phase model, model functions, and model parameters used for simulations of self-organized traffic are presented in Tables I, II, and III, respectively. In the model, discretized and dimensionless length (space coordinate), speed, and

TABLE I: Discrete version of stochastic three-phase traffic flow model for single-lane road

$$\begin{aligned}
 v_{n+1} &= \max(0, \min(v_{\text{free}}, \tilde{v}_{n+1} + \xi_n, v_n + a_{\text{max}}\tau, v_{s,n})), \\
 x_{n+1} &= x_n + v_{n+1}\tau, \\
 \tilde{v}_{n+1} &= \max(0, \min(v_{\text{free}}, v_{s,n}, v_{c,n})), \\
 v_{c,n} &= \begin{cases} v_{c,n}^{(1)} & \text{at } \Delta v_n + a_{\ell,n}\tau < \Delta v_a, \\ v_{c,n}^{(2)} & \text{at } \Delta v_n + a_{\ell,n}\tau \geq \Delta v_a, \end{cases} \\
 v_{c,n}^{(1)} &= \begin{cases} v_n + \Delta_n^{(1)} & \text{at } g_n \leq G_n, \\ v_n + a_n\tau & \text{at } g_n > G_n, \end{cases} \\
 \Delta_n^{(1)} &= \max(-b_n\tau, \min(a_n\tau, v_{\ell,n} - v_n)), \\
 v_{c,n}^{(2)} &= v_n + \Delta_n^{(2)}, \\
 \Delta_n^{(2)} &= k_a a_n \tau \max(0, \min(1, \gamma(g_n - v_n\tau))), \\
 g_n &= x_{\ell,n} - x_n - d, \\
 \Delta v_n &= v_{\ell,n} - v_n, \quad a_{\ell,n} = (v_{\ell,n} - v_{\ell,n-1})/\tau, \\
 a_{\text{max}} &= \begin{cases} a & \text{at } \Delta v_n + a_{\ell,n}\tau < \Delta v_a, \\ k_a a & \text{at } \Delta v_n + a_{\ell,n}\tau \geq \Delta v_a, \end{cases} \\
 v_{\text{free}}, d, a, \Delta v_a, k_a, \text{ and } \gamma &\text{ are constants; } \tau = 1; \\
 \ell &\text{ marks the preceding vehicle.}
 \end{aligned}$$

acceleration are used, which are measured respectively in discretization values $\delta x = 0.01$ m, $\delta v = 0.01$ ms⁻¹, and $\delta a = 0.01$ ms⁻²; the value τ is assumed to be dimensionless value $\tau = 1$. With the exception of the mechanism of a stronger acceleration discussed in Sec. II B, the physics of the model has been explained in the book [17].

TABLE II: Functions used in three phase model

<p>Stochastic time delay of acceleration and deceleration:</p> $a_n = a\Theta(P_0 - r_1), \quad b_n = a\Theta(P_1 - r_1),$ $P_0 = \begin{cases} p_0 & \text{if } S_n \neq 1 \\ 1 & \text{if } S_n = 1, \end{cases} \quad P_1 = \begin{cases} p_1 & \text{if } S_n \neq -1 \\ p_2 & \text{if } S_n = -1, \end{cases}$ $S_{n+1} = \begin{cases} -1 & \text{if } \tilde{v}_{n+1} < v_n \\ 1 & \text{if } \tilde{v}_{n+1} > v_n \\ 0 & \text{if } \tilde{v}_{n+1} = v_n, \end{cases}$ <p>$r_1 = \text{rand}(0, 1)$, $\Theta(z) = 0$ at $z < 0$ and $\Theta(z) = 1$ at $z \geq 0$, $p_0 = p_0(v_n)$, $p_2 = p_2(v_n)$, p_1 is constant.</p> <p>Model speed fluctuations:</p> $\xi_n = \begin{cases} \xi_a & \text{if } S_{n+1} = 1 \\ -\xi_b & \text{if } S_{n+1} = -1 \\ \xi^{(0)} & \text{if } S_{n+1} = 0, \end{cases}$ $\xi_a = a^{(a)}\tau\Theta(p_a - r), \quad \xi_b = a^{(b)}\tau\Theta(p_b - r),$ $\xi^{(0)} = a^{(0)}\tau \begin{cases} -1 & \text{if } r \leq p^{(0)} \\ 1 & \text{if } p^{(0)} < r \leq 2p^{(0)} \text{ and } v_n > 0 \\ 0 & \text{otherwise,} \end{cases}$ <p>$r = \text{rand}(0, 1)$; $a^{(b)} = a^{(b)}(v_n)$; $p_a, p_b, p^{(0)}, a^{(a)}, a^{(0)}$ are constants.</p> <p>Synchronization gap G_n and safe speed $v_{s,n}$:</p> $G_n = G(v_n, v_{\ell,n}),$ $G(u, w) = \max(0, \lfloor k\tau u + a^{-1}\phi_0 u(u - w) \rfloor),$ $v_{s,n} = \min(v_n^{(\text{safe})}, g_n/\tau + v_{\ell}^{(a)}), \quad v_n^{(\text{safe})} = \lfloor v^{(\text{safe})}(g_n, v_{\ell,n}) \rfloor,$ $v^{(\text{safe})}\tau_{\text{safe}} + X_d(v^{(\text{safe})}) = g_n + X_d(v_{\ell,n}),$ $X_d(u) = b\tau^2 \left(\alpha\beta + \frac{\alpha(\alpha-1)}{2} \right), \quad \alpha = \lfloor u/b\tau \rfloor, \quad \beta = u/b\tau - \alpha,$ $v_{\ell}^{(a)} = \max(0, \min(v_{\ell,n}^{(\text{safe})}, v_{\ell,n}, g_{\ell,n}/\tau) - a\tau),$ <p>τ_{safe} is a safe time gap; $b, k > 1$, and ϕ_0 are constants; $\lfloor z \rfloor$ denotes the integer part of a real number z.</p>

TABLE III: Model parameters for three-phase model used in simulations

$$\begin{aligned}
 \tau_{\text{safe}} &= \tau = 1, \quad d = 7.5 \text{ m}, \\
 v_{\text{free}} &= 15.278 \text{ ms}^{-1} \text{ (55 km/h)}, \\
 b &= 1 \text{ ms}^{-2}, \quad a = 0.5 \text{ ms}^{-2}, \\
 k &= 3, \quad \phi_0 = 1, \quad \Delta v_a = 2 \text{ ms}^{-1}, \quad k_a = 4, \quad \gamma = 1, \\
 p_b &= 0.1, \quad p_a = 0.03, \quad p_1 = 0.35, \quad p^{(0)} = 0.005, \\
 p_2(v_n) &= 0.48 + 0.32\Theta(v_n - v_{21}), \\
 p_0(v_n) &= 0.667 + 0.083 \min(1, v_n/v_{01}), \\
 v_{01} &= 6 \text{ ms}^{-1}, \quad v_{21} = 7 \text{ ms}^{-1}. \\
 a^{(a)} &= a, \quad a^{(0)} = 0.2a, \quad a^{(b)}(v_n) = 0.2a + \\
 &+ 0.8a \max(0, \min(1, (v_{22} - v_n)/\Delta v_{22})), \\
 v_{22} &= 7 \text{ ms}^{-1}, \quad \Delta v_{22} = 2 \text{ ms}^{-1}.
 \end{aligned}$$

Appendix C: Two-phase microscopic stochastic traffic flow model for signal-lane road

Rules of vehicle motion in two-phase model, model functions, and model parameters used for simulations of self-organized traffic are presented in Tables IV and V, respectively.

-
- [1] F.V. Webster. Road Research Technical Paper No. 39, Road Research Laboratory, London, UK (1958).
 - [2] J.T. Morgan and J.D.C. Little. Oper. Res. **12**, 896–912 (1964).
 - [3] G.F. Newell. Annals of Math. Stat. **31**, 589–597 (1960).
 - [4] G.F. Newell. SIAM Review. **575**, 223–240 (1965).
 - [5] J.D.C. Little. Oper. Res. **14**, 568–594 (1966).
 - [6] D.I. Robertson. TRRL Report No. LR 253, Transportation and Road Research Laboratory,

TABLE IV: Discrete version of stochastic two-phase traffic flow model for single-lane road

$$\begin{aligned}
 v_{n+1} &= \max(0, \min(v_{\text{free}}, \tilde{v}_{n+1} + \xi_n, v_n + a_{\text{max}}\tau, v_{s,n})) \\
 x_{n+1} &= x_n + v_{n+1}\tau, \\
 \tilde{v}_{n+1} &= \max(0, \min(v_{\text{free}}, v_{s,n}, v_{c,n})), \\
 v_{c,n} &= \begin{cases} v_n + a_n\tau & \text{at } \Delta v_n + a_{\ell,n}\tau < \Delta v_a, \\ v_n + \Delta_n^{(2)} & \text{at } \Delta v_n + a_{\ell,n}\tau \geq \Delta v_a, \end{cases} \\
 \Delta_n^{(2)} &= k_a a_n \tau \max(0, \min(1, \gamma(g_n - v_n\tau))), \\
 g_n &= x_{\ell,n} - x_n - d, \quad \Delta v_n = v_{\ell,n} - v_n, \\
 a_{\ell,n} &= (v_{\ell,n} - v_{\ell,n-1})/\tau, \\
 a_{\text{max}} &= \begin{cases} a & \text{at } \Delta v_n + a_{\ell,n}\tau < \Delta v_a, \\ k_a a & \text{at } \Delta v_n + a_{\ell,n}\tau \geq \Delta v_a, \end{cases} \\
 v_{\text{free}}, d, a, \Delta v_a, k_a, & \text{ and } \gamma \text{ are constants; } \tau = 1; \\
 \ell & \text{ marks the preceding vehicle.}
 \end{aligned}$$

Crowthorne, UK (1969).

- [7] D.I. Robertson. In: Proceedings of the International Symposium on Traffic Control Systems, pp. 262–288 (1979).
- [8] P.B. Hunt, D.I. Robertson, R.D. Bretherton, and R.I. Winton. TRRL Report No. LR 1014, Transp. and Road Res. Lab., Crowthorne, UK (1981).
- [9] P.G. Michalopoulos, G. Stephanopoulos, G., Stephanopoulos. Transp. Res. B **15**, 35–51 (1981).
- [10] V.B. Pisharody. Transp. Sc. **14**, 9–41 (1980).
- [11] G. Stephanopoulos, P.G. Michalopoulos. Transp. Res. A **13**, 295–307 (1979).
- [12] N.H. Gartner. Transp. Res. Rec. **906** 75–81 (1983).
- [13] R.B. Grafton, G.F. Newell. In: Vehicular Traffic Science (Editors: L C. Edie, R. Herman and R. Rothery). Elsevier, New York, 239–257 (1967).
- [14] W.R. McShane, R.P. Roess. Traffic Engineering (Prentice Hall, Englewood Cliffs, NJ, 1990).
- [15] N.H. Gartner, Ch. Stamatiadis, in *Encyclopedia of Complexity and System Science*, ed. by R.A. Meyers. (Springer, Berlin, 2009), pp. 9470-9500.
- [16] F. Dion, H. Rakha, Y.S. Kang, Transp. Res. B, **38**, 99–122 (2004).

TABLE V: Functions and parameters for two-phase model used in simulations

<p style="text-align: center;">Stochastic time delay of acceleration and deceleration:</p> $a_n = a\Theta(P_0 - r_1), \quad P_0 = \begin{cases} p_0 & \text{if } S_n \neq 1 \\ 1 & \text{if } S_n = 1, \end{cases}$ $S_{n+1} = \begin{cases} -1 & \text{if } \tilde{v}_{n+1} < v_n \\ 1 & \text{if } \tilde{v}_{n+1} > v_n \\ 0 & \text{if } \tilde{v}_{n+1} = v_n, \end{cases}$ <p>$r_1 = \text{rand}(0, 1)$, $\Theta(z) = 0$ at $z < 0$ and $\Theta(z) = 1$ at $z \geq 0$, $p_0 = p_0(v_n)$.</p> <p style="text-align: center;">Model speed fluctuations:</p> $\xi_n = \begin{cases} -\xi_b & \text{if } S_{n+1} = -1 \\ \xi^{(0)} & \text{if } S_{n+1} = 0, \end{cases}$ $\xi_b = a^{(b)}\tau\Theta(p_b - r),$ $\xi^{(0)} = a^{(0)}\tau \begin{cases} -1 & \text{if } r \leq p^{(0)} \\ 0 & \text{otherwise,} \end{cases}$ <p>$r = \text{rand}(0, 1)$; $a^{(b)} = a^{(b)}(v_n)$; $p_b, p^{(0)}, a^{(0)}$ are constants.</p> <p>Safe speed $v_{s,n}$ as well as the model parameters and functions $v_{\text{free}}, d, a, k_a, \gamma, p_0 = p_0(v_n)$, $a^{(b)} = a^{(b)}(v_n), p_b, p^{(0)}, a^{(0)}$ are the same as those in three phase model (Tables II and III).</p>

- [17] B.S. Kerner. *The Physics of Traffic* (Springer, Berlin, New York 2004).
- [18] B.S. Kerner. *Introduction to Modern Traffic Flow Theory and Control*. (Springer, Berlin, New York, 2009).
- [19] B.S. Kerner. Phys. Rev. E **84**, 045102(R) (2011).
- [20] B.S. Kerner, S.L. Klenov, Phys. Rev. E **68** 036130 (2003).
- [21] Definitions and features of three-phase theory initially developed for highway traffic [22, 23] can be found in [17, 18]. Over time a number of different models and results in the framework of three-phase theory have been developed (e.g., [24–64]).

- [22] B.S. Kerner, in *Proceedings of the 3rd Symposium on Highway Capacity and Level of Service*, ed. by R. Rysgaard. Vol 2 (Road Directorate, Ministry of Transport – Denmark, 1998), pp. 621–642; In *Traffic and Granular Flow' 97*, ed. by M. Schreckenberg, D.E. Wolf. (Springer, Singapore, 1998), pp. 239–267; In *Transportation and Traffic Theory*, ed. by A. Ceder. (Elsevier Science, Amsterdam 1999), pp. 147–171.
- [23] B.S. Kerner. Phys. Rev. Lett. **81**, 3797 (1998); Trans. Res. Rec. **1678**, 160–167 (1999); Physics World **12** (8), 25–30 (August 1999).
- [24] B.S. Kerner, S.L. Klenov, J. Phys. A: Math. Gen. **35**, L31–L43 (2002).
- [25] B.S. Kerner, S.L. Klenov, D.E. Wolf, J. Phys. A: Math. Gen. **35**, 9971–10013 (2002).
- [26] L.C. Davis Phys. Rev. E **69** 016108 (2004).
- [27] H.K. Lee, R. Barlović, M. Schreckenberg, D. Kim. Phys. Rev. Lett. **92**, 238702 (2004).
- [28] R. Jiang, Q.-S. Wu. J. Phys. A: Math. Gen. **37** 8197–8213 (2004).
- [29] B.S. Kerner, S.L. Klenov, J. Phys. A: Math. Gen. **37**, 1–36 (2004).
- [30] B.S. Kerner, S.L. Klenov. J. Phys. A: Math. Gen. **39**, 1775–1809 (2006).
- [31] K. Gao, R. Jiang, S.-X. Hu, B.-H. Wang, Q.-S. Wu. Phys. Rev. E **76** 026105 (2007).
- [32] L.C. Davis. Physica A **368** 541–550 (2006).
- [33] L.C. Davis. Physica A **361** 606–618 (2006).
- [34] L.C. Davis. Physica A **387** 6395–6410 (2008).
- [35] L.C. Davis. Physica A **388** 4459–4474 (2009).
- [36] L.C. Davis. Physica A **389** 3588–3599 (2010).
- [37] L.C. Davis. Physica A **391**, 1679 (2012).
- [38] R. Jiang, M.-B. Hua, R. Wang, Q.-S. Wu. Phys. Lett. A **365** 6–9 (2007).
- [39] R. Jiang, Q.-S. Wu. Phys Rev E **72** 067103 (2005).
- [40] R. Jiang, Q.-S. Wu. Physica A **377** 633–640 (2007).
- [41] R. Wang, R. Jiang, Q.-S. Wu, M. Liu. Physica A **378** 475–484 (2007).
- [42] A. Pottmeier, C. Thiemann, A. Schadschneider, M. Schreckenberg. In: A. Schadschneider, T. Pöschel, R. Kühne, M. Schreckenberg, D.E. Wolf (eds). *Traffic and Granular Flow'05*, (Springer, Berlin, 2007) pp. 503–508.
- [43] X.G. Li, Z.Y. Gao, K.P. Li, X.M. Zhao. Phys Rev E **76** 016110 (2007).
- [44] B.S. Kerner, S.L. Klenov, and A. Brakemeier, arXiv: 0712.2711 (2007).
- [45] B.S. Kerner, S.L. Klenov, and A. Brakemeier, Proc. of 2008 IEEE Intelligent Vehicles Sym-

- posium, pp. 180–185 (2008); Proc. of 4th Int. Workshop V2VCOM 2008, pp. 57–63 (2008); B.S. Kerner, S.L. Klenov, and A. Brakemeier. E-print, arXiv:0910.0381v2 (2009); Traf. Eng. & Cont. No. 6, 217–222 (2010); In: Proceedings of the Transportation Research Board 2010 Annual Meeting (TRB, Washington DC, 2010), Paper No.: 10-0456; B.S. Kerner, e-print: arXiv1012.5159 (2010); R.-P. Schäfer, S. Lorkowski, N. Witte, J. Palmer, H. Rehborn, B.S. Kerner. Traf. Eng. and Cont. **52**, No. 5, 225–230 (2011); B.S. Kerner, H. Rehborn, J. Palmer, S.L. Klenov. Traf. Eng. and Cont. **52**, No. 3, 141–148 (2011); B.S. Kerner, H. Rehborn, R.-P. Schäfer, S.L. Klenov, J. Palmer, S. Lorkowski, N. Witte. Physica A, DOI: 10.1016/j.physa.2012.07.070 (2012).
- [46] J.J. Wu, H.J. Sun, Z.Y. Gao. Phys Rev E **78** 036103 (2008).
- [47] K. Gao, R. Jiang, B.-H. Wang, Q.-S. Wu. Physica A **388** 3233–3243 (2009).
- [48] B. Jia, X.-G. Li, T. Chen, R. Jiang, Z.-Y. Gao. Transportmetrica **7**, 127 (2011).
- [49] J.-F. Tian, B. Jia, X.-G. Li, R. Jiang, X.-M. Zhao, Z.-Y. Gao. Physica A **388** 4827–4837 (2009).
- [50] S. He, W. Guan, L. Song. Physica A **389** 825–836 (2009).
- [51] Ch.-J. Jin, W. Wang, R. Jiang, K. Gao, J. Stat. Mech. **2010**, P03018 (2010).
- [52] S. Kokubo, J. Tanimoto, A. Hagishima. Physica A **390** 561–568 (2011).
- [53] H.-K. Lee, B.-J. Kim, Physica A **390**, 4555–4561 (2011).
- [54] Ch.-J. Jin, W. Wang, Physica A **390**, 4184–4191 (2011).
- [55] J.P.L. Neto, M.L. Lyra, C.R. da Silva, Physica A **390**, 3558–3565 (2011).
- [56] P. Zhang, Ch.-X. Wu, S.C. Wong, Physica A, **391**, 456 (2012).
- [57] B.S. Kerner, S.L. Klenov, M. Schreckenberg Phys. Rev. E **84**, 046110 (2011).
- [58] B. S. Kerner, Physica A **355** 565–601 (2005); IEEE Trans. on Intel. Trans. Sys. **8** 308–320 (2007); Traffic Engineering and Control **48** 28 (2007); 66; 114; Trans. Res. Rec. **1999** 30–39 (2007); Trans. Res. Rec. **2088** 80–89 (2008).
- [59] S. Lee, B. Heydecker, Y. H Kim, E.-Y. Shon, J. of Adv. Trans. **4**, 143–158 (2011).
- [60] J.-F. Tian, Z.-Z. Yuana, M. Treiber, B. Jia, W.-Y. Zhanga, Physica A **391**, 3129 (2012).
- [61] M.E.M. Kimathi, Mathematical Models for 3-Phase Traffic Flow Theory, Doctor Thesis (2012), <https://kluedo.ub.uni-kl.de/frontdoor/index/index/docId/2899>.
- [62] R. Borsche, M.E.M. Kimathi, A. Klar, Comp. and Math. with Appl. (to appear).
- [63] Y. Wang, Y.I. Zhang, J. Hu, L. Li, Int. J. of Mod. Phys. C **23** 1250060 (2012).

- [64] J.-f. Tian, Z.-z. Yuan, B. Jia, H.-q. Fan, T. Wang, Phys. Lett. A **376**, 2781–2787 (2012).
- [65] Time step $\tau = 1$ s is consistent with any small values of time parameters of green wave, e.g., with possible small values of ΔT_b and ΔT_e . This is because time step is associated with a time-discrete *update* of the speed and acceleration of a vehicle only, while between any two subsequent time steps vehicles move continuously in time. However, the choice of time step limits maximum flow rate, e.g., the maximum value q_{GW} that can be given at $x = x_b$.
- [66] The increase in maximum acceleration from standstill does not influence on safety motion of following vehicles because vehicles accelerate after a time delay in acceleration whose mean value (about 1.74 s) remains the same as that in the former model [17].
- [67] B.S. Kerner, S.L. Klenov, Phys. Rev. E **80** 056101 (2009).
- [68] B.S. Kerner, S.L. Klenov, J. Phys. A: Theor. Math. **43** 425101 (2010).
- [69] B.S. Kerner, S.L. Klenov, A. Hiller, J. Phys. A: Math. Gen. **39**, 2001–2020 (2006).
- [70] B.S. Kerner, S.L. Klenov, A. Hiller, H. Rehborn, Phys. Rev. E **73**, 046107 (2006).
- [71] In over-saturated traffic, moving queues can propagate many kilometers upstream during the time interval $T_{ob} = 60$ min. To avoid a dependence of simulation results on upstream boundary conditions, a long road section $x_{LS} - x_b = 11$ km is chosen for those model parameters at which speed disturbances that initiate the breakdown occur in a small neighborhood of the light signal location, i.e., disturbances occurring away of the light signal location(s) are negligible for the breakdown. To make associated figures clear, simulated road section $x_b \leq x \leq 6$ km is not shown. This explains the value $x = x_{LS} = 5$ km shown in related figures. The exception is the case of green waves with $\Delta T_b^{(ideal)} = 8$ s for which in figures road co-ordinates are the same as those in simulations.
- [72] Simulations show that if the flow rate q_{GW} is slightly increased in comparison with used in Fig. 3, then MSP occurs in each of the cycles. This is because the initial disturbance becomes larger than the critical one in each of the cycles. Otherwise, when q_{GW} is slightly decreased, then probability of MSP occurrence decreases sharply.
- [73] Note that different simulation realizations (runs) are made at the same chosen $q_{in}(t)$ and parameters of the light signal. The only difference between these runs are different initial numbers for random value r used in functions $rand()$ of the model (see Appendix B) at time $t = 0$ that leads to different *initial conditions* for model fluctuations in the different runs.
- [74] This is crucially different from the cases in which condition (5) is not satisfied (Sec. IID):

Then a large enough local disturbance leading to MSP emergence appears *always* in a small neighborhood of the light signal location. Much smaller speed disturbances occurring along the green wave away from the light signal are usually negligible for the green wave breakdown; this is because growing small speed disturbances leave the green wave before they become comparable with the MSPs shown in Fig. 3 (d, e).

- [75] Probability $P^{(B)}$ that traffic breakdown at the light signal occurs spontaneously during the time interval T_{ob} is found through formula $P^{(B)} = n_b/N_r$, where N_r is the number of different realizations (runs) [73], n_b is the number of runs in which traffic breakdown has occurred, therefore, $N_r - n_b$ is the number of runs in which no breakdown has occurred. In all simulations, we have used $N_r = 40$.
- [76] We have also found that sometimes at a given value M_{turn} in some realizations (runs) [73] the breakdown does occur; however, in other realizations during a few following light signal cycles the initial disturbance decays fully, i.e., no breakdown occurs.
- [77] A smoothing character of function $P^{(B)}(\bar{q}_{in})$ around $\bar{q}_{in} = C_{min}$ for the red wave (Fig. 10 (g)) is caused by the effect of model fluctuations on queue discharge outflow.
- [78] B.S. Kerner, J. Phys. A: Math. Theor. **44**, 092001 (2011).
- [79] B.S. Kerner, Traffic Engineering and Control **52**, Nr. 9, 379 (2011).
- [80] B.S. Kerner, in: 2011 IEEE Forum on Integrated and Sustainable Transportation Systems Vienna, Austria, June 29 - July 1, Paper Nr. 0023 (2011), pp. 196–201.
- [81] There is a range of small flow rates \bar{q}_{in} close to C_{min} within which no synchronized flow states S_2 on the double Z-characteristic occur (Fig. 12 (d)). To induced the green wave breakdown in this case, a large number of vehicles M_{turn} leading to a long queue at the light signal is needed: A long queue discharge should cause a stop of *all vehicles* within the following green wave, i.e., a direct F→J transition.
- [82] For example, if link inflow with the rate q_m consists of “fast”, “slow”, and “long” vehicles with percentages f_m , s_m , and l_m (where $f_m + s_m + l_m = 100\%$), then $\zeta_m = (f_m, s_m, l_m)$.
- [83] When the bottleneck w is caused by the light signal, then $\alpha_w = \alpha_w(\vartheta_w, \nu_w, \beta_w, \varphi_w, \mu_w)$, where ϑ_w is a cycle length of the light signal w , ν_w is the offsets, i.e., the difference of the reference point of the respective local signal timing plan to the global (network-wide) time scale reference point of the light signal phase begin, β_w defines the succession of the phases, parameters φ_w and μ_w define the start times and durations of the green and red phases for the light signal.

- [84] The exception is a very heavy highway bottleneck (see B.S. Kerner, *J. Phys. A: Math. Theor.* **41** 215101 (2008)).
- [85] B.S. Kerner, P. Konhäuser, *Phys. Rev. E* **48**, 2335–2338 (1993); *Phys. Rev. E* **50**, 54–83 (1994); S. Krauß, P. Wagner, C. Gawron, *Phys. Rev. E* **55**, 5597–5602 (1997); R. Barlović, L. Santen, A. Schadschneider, M. Schreckenberg, *Eur. Phys. J. B* **5**, 793–800 (1998); D. Chowdhury, L. Santen, A. Schadschneider, *Physics Reports* **329**, 199 (2000); D. Helbing, *Rev. Mod. Phys.* **73**, 1067–1141 (2001); T. Nagatani, *Rep. Prog. Phys.* **65**, 1331–1386 (2002); K. Nagel, P. Wagner, R. Woesler, *Operation Res.* **51**, 681–716 (2003); R. Mahnke, J. Kaupužs, I. Lubashevsky, *Phys. Rep.* **408**, 1-130 (2005).